

---

# 4 Estimation Techniques for Phase Equilibria of Natural Gas Hydrates

## INTRODUCTION

Substantially different from ice, the phase equilibria of natural gas hydrates represents the most important set of hydrate properties. In contrast to kinetic phenomena, hydrate phase equilibria are well defined and determine a boundary to the kinetic problem. This chapter addresses hydrate phase equilibria with approximate methods that provide an understanding of the phenomena involved.

Engineers may ask, “When I plan to use a simulation package such as ASPEN PLUS™, PRO II™, UNISIM™, or even the CD provided with this book, why should I be concerned with simpler, less accurate methods of phase equilibria and diagrams? If I’m concerned with accuracy, why not use two prediction packages and compare the result?”

The answer addresses one of the key modern engineering dilemmas, that of providing engineering judgment to evaluate calculations from “black-box” complex computer codes. Computer programs may provide a number that may not be a good model of physical reality. The simpler methods in this chapter are very valuable, first for intuitive understanding and second to provide both a first estimation and a check of more complex calculations.

As one step toward understanding phase equilibria, the rigorous phase diagrams of the first edition have been greatly simplified, and those of the second edition have been corrected via recent experiments. Those who deal with gas production, transportation, and high temperature processing should find greater utility in these diagrams, which are restricted to the region above 0°F. However, gas processors dealing with lower, cryogenic temperatures may wish to refer to the first edition (1989) [or to [Harmens and Sloan, \(1990\)](#) or to [Wierzchowski and Monson, \(2006\)](#)] for more comprehensive phase diagrams.

At the conclusion of this chapter, the engineer should be able to answer questions such as the following:

1. What are pressure–temperature–composition bounds on sI and sII hydrate formation?
2. What is a typical pressure–temperature phase diagram for sH hydrates?
3. What rapid calculations can be made to check the prediction of a computer simulation?

4. What is a quick estimate of the thermodynamic inhibitor effect?
5. What are the accuracy limits of hydrate hand calculation methods?
6. How much heat is necessary to dissociate hydrates?

Just as engineering is sometimes considered to be an applied science, the concepts of this chapter should provide for applications—to hydrates in the earth ([Chapter 7](#)) and to hydrate problems in production, transportation, and processing of oil and natural gas ([Chapter 8](#)). As an introduction to the chapter, consider an example of some typical hydrate calculations.

---

### Example 4.1: Estimates of Hydrate Formation Conditions

An engineer (or researcher) wishes to predict hydrate formation pressures of single guests of methane ( $\text{CH}_4$ ) and of propane ( $\text{C}_3\text{H}_8$ ) at 278.2 K, and to determine how those pressures would be affected by changing the gas composition to 95.6 mol%  $\text{CH}_4$  + 4.4%  $\text{C}_3\text{H}_8$ .

#### *Some Solution Methods*

1. For simple  $\text{C}_3\text{H}_8$  hydrates, the engineer could review the  $P$ - $T$  phase diagram such as that shown in [Figure 4.1](#) (reproduced from [Figure 1.2](#)) and note the regions of hydrate formation. He might then draw a straight line between the lower and upper quadruple points ( $Q_1$  and  $Q_2$  in [Table 4.2](#)) to obtain a semilogarithmic plot of pressure versus the absolute temperature, as shown in Figure 4.1. The pressure may be semilogarithmically interpolated to obtain a pressure of 0.46 MPa at 278.2 K. For  $\text{CH}_4$ , however, there is no upper quadruple point on the  $P$ - $T$  phase diagram, so this technique is not available.
2. For  $\text{CH}_4$  hydrates, the engineer may turn to an Antoine-like relation ( $\ln P = a + b/T$ , with constants in [Table 4.1](#)) to calculate a hydrate formation pressure of 4.04 MPa. A corresponding value for  $\text{C}_3\text{H}_8$  at 278.2 K is calculated as 0.54 MPa, slightly different from the value of 0.46 obtained in method 1. Note that solution methods 1 and 2 imply a semilogarithmic correlation for single guest hydrates.
3. These simple hydrate predictions compare well with the data of Thakore and Holder (1987) at 4.5 and 0.51 MPa for  $\text{CH}_4$  and  $\text{C}_3\text{H}_8$ , respectively, at 278.2 K.
4. For the mixture of 95.6%  $\text{CH}_4$  + 4.4%  $\text{C}_3\text{H}_8$ , a first approach would be a linear or semilogarithmic, compositional interpolation of the mixture formation pressure at 278.2 K, but those values are 4.3 and 4.1 MPa, respectively, both of which are in error by 300%.
5. For accurate mixture formation pressure estimation, a simple phase diagram or Antoine-like equation does not exist, but the engineer may use the gas gravity chart ([Figure 1.4](#)) to approximate the phase

equilibrium condition, as detailed in Section 4.2.1. The gas gravity is 0.596 and the formation pressure is predicted as 1.95 MPa. (See [Section 4.2.1](#) for details and examples of this calculation.)

6. If a better estimate of the mixture formation pressure is needed, the engineer may use the  $K_{vsi}$  value method in Section 4.2.2 to obtain an estimated hydrate pressure of 1.26 MPa.
7. The engineer may finally turn to the computer simulation packages mentioned above to obtain a mixture hydrate dissociation pressure of 1.26 MPa.
8. The final test of such mixture calculations is comparison with data. In this case, the mixture hydrate formation pressure at 278.2 K was measured by Thakore and Holder (1987) as 1.30 MPa. Note that the small amount of C<sub>3</sub>H<sub>8</sub> (4.4%) caused the mixture dissociation pressure (1.3 MPa) to be closer to that of simple C<sub>3</sub>H<sub>8</sub> (0.50 MPa) than that of CH<sub>4</sub> (4.31 MPa). Note also that the  $K_{vsi}$  method generated in 1942 provides a result comparable to that of the modern computer method.

The above example illustrates that the determination of simple (one guest) hydrate formation from water and gas has been experimentally established with a high degree of certainty. However, an infinite number of mixture hydrate possibilities exist for the eight sI and sII hydrate formers in natural gas (CH<sub>4</sub>, C<sub>2</sub>H<sub>6</sub>, C<sub>3</sub>H<sub>8</sub>, i-C<sub>4</sub>H<sub>10</sub>, n-C<sub>4</sub>H<sub>10</sub>, CO<sub>2</sub>, H<sub>2</sub>S, N<sub>2</sub>). In the three-phase region, the prediction methods are easily justified by the large effort and expense to obtain hydrate data.

---

Hydrate phase diagrams for water–hydrocarbon systems provide a convenient overview of the calculation types. These diagrams differ substantially from the normal hydrocarbon phase diagrams primarily due to hydrates and the hydrogen bonds inherent in aqueous systems. The phase diagrams of Section 4.1 provide an overview for the calculation methods in this chapter and the next.

Section 4.2 deals with the most useful hydrate equilibria—calculations of temperatures and pressures at which hydrates form from gas and free water. In this section, two historical methods, namely, the gas gravity method (Section 4.2.1) and the  $K_{vsi}$  value method (Section 4.2.2), for calculating the pressure–temperature equilibrium of three phases (liquid water–hydrate–vapor, L<sub>w</sub>–H–V)<sup>1</sup> are discussed. With the gas gravity method in Section 4.2.1.1, a method is given for limits to expansion, as for flow through a valve. In Section 4.2.2 a distribution coefficient ( $K_{vsi}$ ) method is provided to determine whether a component prefers residing in the hydrate or the vapor phase. These methods provide initial estimates for the calculation and provide a qualitative understanding of the equilibria. A statistical

---

<sup>1</sup> Phase (and abbreviation) nomenclature given in order of decreasing water concentration in each phase.

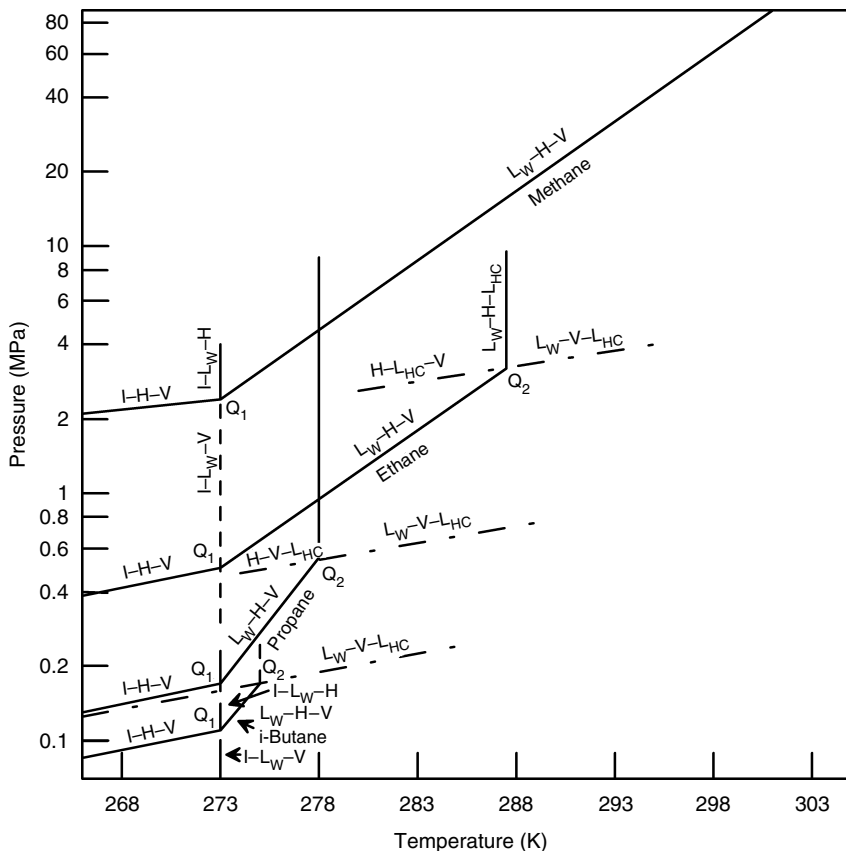


**FIGURE 4.1** Phase diagrams for some simple natural gas hydrocarbons that form hydrates. Q<sub>1</sub>: lower quadruple point, Q<sub>2</sub>: upper quadruple point. (Modified, from Katz, D.L., Cornell, D., Kobayashi, R., Poettman, F.H., Vary, J.A., Elenbaas, J.R., Weinaug, C.F., *Handbook of Natural Gas Engineering* (1959). With permission from McGraw-Hill.)

thermodynamic method provides the best three-phase calculation; however, because it is both more comprehensive and detailed, it is relegated to Chapter 5. Because the discovery of structure H (Ripmeester et al., 1987) was more recent compared to sI/sII there are no approximate methods for pressure and temperature phase equilibrium in the current chapter, but the statistical mechanics method is applied to that structure in Chapter 5, obviating the approximate methods.

The two calculation methods in Section 4.2 enable prediction of the three-phase (L<sub>w</sub>-H-V) gas mixture region extending between the two quadruple points Q<sub>1</sub> and Q<sub>2</sub> in Figure 4.1. Section 4.3 provides a method to use the techniques of Section 4.2 to locate both quadruple points on a pressure-temperature plot. Section 4.3 also discusses equilibrium of three condensed phases [aqueous liquid-hydrate-hydrocarbon liquid (L<sub>w</sub>-H-L<sub>HC</sub>)]. Determination of equilibrium from condensed phases provides an answer to the question, “Given a liquid

**TABLE 4.1****Hydrate Formation for Three-Phase Conditions of Single Natural Gas Components, Using  $P$  [kPa] =  $\exp(a + b/T$  [K])**

Component	Type	T range (°C)	a	b
Methane	L <sub>W</sub> -H-V	0 to 25	38.980	-8533.80
Methane	I-H-V	-25 to 0	14.717	-1886.79
Ethane	L <sub>W</sub> -H-V	0 to 14	44.273	-10424.25
Ethane	I-H-V	-25 to 0	17.511	-3104.54
Propane	L <sub>W</sub> -H-V	0 to 5	67.130	-16921.84
Propane	I-H-V	-25 to 0	17.156	-3269.65
Isobutane	L <sub>W</sub> -H-V	0 to 1.5	61.740	-15571.43
Isobutane	I-H-V	-25 to 0	18.950	-3887.32
Carbon dioxide	L <sub>W</sub> -H-V	0 to 11	44.580	-10246.28
Carbon dioxide	I-H-V	-25 to 0	18.594	-3161.41
Nitrogen	L <sub>W</sub> -H-V	0 to 25	37.808	-7688.63
Nitrogen	I-H-V	-25 to 0	15.129	-1504.28
Hydrogen sulfide	L <sub>W</sub> -H-V	0 to 25	34.828	-8266.10
Hydrogen sulfide	I-H-V	-25 to 0	16.560	-3270.41

*Source:* From Kamath, V.A., *Study of Heat Transfer Characteristics During Dissociation of Gas Hydrates in Porous Media*, Ph.D. Dissertation University of Pittsburgh, University Microfilms No. 8417404, Ann Arbor, MI, 1984. With permission.

hydrocarbon, without gas, and a free water phase, at what pressure and temperature will hydrates form?" The structure H exception is considered in [Chapter 5](#), because, as noted in [Chapter 2](#), the large guest molecule required is a liquid, while the small molecule is a gas at ambient conditions.

The inhibition of three-phase hydrate formation is discussed in [Section 4.4](#). These predictions enable answers to such questions as, "How much methanol (or other inhibitor) is required in the free water phase to prevent hydrates at the pressures and temperatures of operation?" Classical empirical techniques such as that of Hammerschmidt (1934) are suitable for hand calculation and provide a qualitative understanding of inhibitor effects. It should be noted that only thermodynamic inhibitors are considered here. The new low-dosage hydrate inhibitors [LDHIs, such as kinetic inhibitors (KIs) or antiagglomerants (AAs)] do not significantly affect the thermodynamics but the kinetics of hydrate formation; LDHIs are considered in [Chapter 8](#).

The calculation of two-phase (hydrate and one other fluid phase) equilibrium is discussed in [Section 4.5](#). The question, "To what degree should hydrocarbon gas or liquid be dried in order to prevent hydrate formation?" is addressed through these equilibria. Another question addressed in [Section 4.5](#) is, "What mixture solubility in water is needed to form hydrates?"

Finally, [Section 4.6](#) concerns the relationship of phase equilibrium to other hydrate properties. The hydrate application of the Clapeyron equation is discussed

with regard to calculating heats of formation and the hydrate number. Other techniques for determining the hydrate number are also discussed.

The calculation methods in this chapter and the next should be taken only as estimates, within the accuracy limits cited. Since predictions are only as good as available experimental data, when questions arise, the examined data should be taken as reliable and the calculation method questioned. If it were economical to obtain accurate data for each case, that would be preferred. However, at the time of writing this book, the typical cost is a week of effort and \$2000/data point, once the apparatus is calibrated.

## Measurable Variables and Gibbs' Phase Rule: How to Ask a Valid Phase Equilibrium Question

In phase equilibria there are five common types of variables:

1. Pressure
2. Temperature
3. Concentrations of the gas, liquid(s), or hydrate phases
4. Volume or density
5. Phase amounts

In the above list, the pressure and temperature are commonly measured in every process, so it is normal to discuss phase equilibrium in terms of those variables, as will be done in this chapter and the next.

However, engineers normally can access only the concentrations of the water-free hydrocarbon phase, and that of the hydrocarbon-free water/ice phase, rather than the total phase concentrations. Other concentrations are generally difficult to measure, except by unusual techniques. While the concentration of the water-free hydrocarbon phase is readily measured (via chromatography, for example) the water concentration of the hydrocarbon phase is generally so low (typically parts per thousand or less) that sophisticated techniques (dual chromatographic columns, etc.) are required for reliable measurement.

In addition, the water phase usually has very low concentrations of hydrocarbons (ice has none) so that sophisticated techniques are needed to measure the low concentrations of hydrocarbons in water, which are usually much less than 1 mol%. While some scientists may have these instruments available, engineers do not typically have access to such sophisticated measurement techniques.

Similarly, the last two variables in the above list (volume/density and phase amounts) are difficult to measure with commonly available instruments. As a result, hydrate phase equilibria are normally determined in terms of four variables: (1) pressure, (2) temperature, (3) water-free hydrocarbon phase composition, and (4) the free-water phase composition (excluding hydrocarbons but including salts, alcohols, and glycols).

The other variables such as the density, hydrate composition, and phase amounts may be predicted by phase equilibria, and confirmed by a few

measurements that are difficult to obtain and thus not common. For example, as shown in [Chapter 6](#), spectroscopic devices such as NMR or Raman spectroscopy can be used to determine the hydrate composition or hydrocarbons dissolved in water; however, access to NMR or Raman methods are available only in a few laboratories. Similarly, the phase amounts (water, vapor, and hydrate) have only been measured a few times, notably in the laboratory of Tohidi et al. (1994).

Normally, the practicing engineer can specify the water-free hydrocarbon composition, and the amount of inhibitor (salts, alcohols, or glycols) in the free water phase, and would like to predict the three-phase ( $L_w$ -H-V) hydrate formation pressure, given the lowest temperature of the process (or predict the formation temperature, given the highest pressure in the process). Protection at the extreme conditions (lowest  $T$  and highest  $P$ ) helps ensure hydrate protection at the other process conditions.

One essential question is, “How many variables must be specified to obtain a solution unique to the phase equilibrium calculation?” It is possible to have an infinite number of solutions to a problem if too few variables are specified—or no solution if too many variables are specified. One answer to this question is provided by Gibbs’ Phase Rule (Gibbs, 1928, p. 96), simply stated for nonreacting systems by the equation:

$$F = C - P' + 2 \quad (4.0)$$

where

$F$  = the number of intensive variables needed to specify the system

$C$  = the number of components in the system

$P'$  = the number of phases in the system.

An intensive variable [such as the temperature ( $T$ ), pressure ( $P$ ), or individual mole fractions of a single phase ( $x_{si}$ ,  $x_i$ , or  $y_i$  of the hydrate, liquid, or vapor phases, respectively)] is defined as a measured value that is independent of the phase amount. For example,  $T$ ,  $P$ ,  $x_{si}$ ,  $x_i$ ,  $y_i$  or density are intensive variables, while phase masses, volumes, or amounts are extensive variables, and thus not addressed by Gibbs’ Phase Rule.

Consider the potential for hydrate formation from methane gas and free water. One question would be, “At what temperature ( $T$ ) will hydrates form for a given pressure ( $P$ )?” Before the calculation is done, one might wonder if there is a unique solution for the problem, or if the problem is under-specified (has an infinite number of solutions). Since the components are methane and water  $C = 2$ , and the phases are three (L<sub>w</sub>-H-V) by the Gibbs’ Phase Rule, one intensive variable ( $F = 1$ ), such as either  $T$  or  $P$  must be specified in order to obtain a unique solution for the formation of hydrates.

Thus by specifying either  $T$  or  $P$ , there is a unique solution to determine the other intensive variables (such as the  $T$  or  $P$  that was not specified, as well as the other intensive variables listed above). Again, extensive variables such as the volumes or phase amounts are not considered in Gibbs’ Phase Rule.

As a special case of this example, one might specify that a natural gas mixture is in very large excess relative to the water phase (as in a gas-dominated pipeline), so that the gas composition does not change upon hydrate formation. Effectively,  $C = 1$  for the gas components, with an additional component for the water (total  $C = 2$ ). With three phases (L<sub>w</sub>-H-V), there must be one intensive variable ( $F = 2 - 3 + 2$ ) for a constant gas mixture composition (in large excess) relative to the water phase, specifying that the highest pipeline pressure is sufficient to determine the temperature (and the other intensive variables) at which hydrates form with a gas of fixed composition.

On the other hand, if a pure methane (or fixed gas composition) pipeline has no free water but only dissolved water in the gas, an operator may ask, "What is the temperature for a pipeline pressure of 2150 psia, at which hydrates will form without a free water phase?" Because  $C = 2$  (water and fixed gas composition) and  $P' = 2$  (gas and hydrates), there are two intensive variables ( $F = 2 - 2 + 2$ ) required to specify the system; so there is no unique solution, but an infinite number of temperatures can be obtained in the two-phase (H-V) region, when only pressure is specified. A better question would be, "For a methane (or fixed gas composition) pipeline operating at 2150 psia and a water content of 200 ppm what would be the temperature at which hydrates will form?" In this case, two intensive variables ( $P$  and  $y_w$ ) are specified so there is a unique solution.

In the last common condition, for four phases in equilibrium (such as I-L<sub>w</sub>-H-V) at the lower quadruple point, the number of intensive variables must equal the number of components minus two. For a mixture of methane and water (or for a gas mixture in large excess so that the composition does not change) no intensive variables are required—that is, the lower quadruple point is fixed at a unique pressure, temperature, as well as the composition of all the phases.

See [Section 4.1.5](#) for other examples of how Gibbs' Phase Rule works in the methane + water phase diagram. Section 5.2 shows the application of the Gibbs' Phase Rule for hydrate guests of methane, ethane, propane, and their mixtures.

## 4.1 HYDRATE PHASE DIAGRAMS FOR WATER + HYDROCARBON SYSTEMS

The phase behavior of hydrocarbon + water mixtures differs significantly from that of normal hydrocarbon mixtures. Differences arise from two effects, both of which have their basis in hydrogen bonding. First, the hydrate phase is a significant part of all hydrocarbon + water phase diagrams for hydrocarbons with a molecular size lower than 9 Å. Second, water and hydrocarbon molecules are so different that, in the condensed state, two distinct liquid phases form, each with a very low solubility in the other.

For a rigorous discussion of phase diagrams, the reader is referred to Harmens and Sloan (1990) or to Huo et al. (2003), which represent an extension and in some cases a correction to those published earlier by Kobayashi (1951), by Kobayashi in Katz et al. (1959), by Bourrie and Sloan (1986), or in the earlier editions of this

monograph (also see [Section 1.1.3](#)). Recently, Wierzchowski and Monson (2006) provided a molecular simulation of the phase diagram, with an accompanying discussion. The remainder of Section 4.1 provides a qualitative understanding of phase diagrams. Quantitative predictions may be obtained by methods in later sections of this chapter and, most accurately, in [Chapter 5](#).

While a first approach to phase diagrams is given here, Section 5.2 extends the phase diagrams in this portion of Chapter 4 to single, binary, and ternary mixtures of methane, ethane, and propane. The reader may wish to consult Section 5.2 for a more enlightening discussion that applies the van der Waals and Platteeuw method to the most common components of natural gases.

#### 4.1.1 Pressure–Temperature Diagrams of the $\text{CH}_4 + \text{H}_2\text{O}$ (or $\text{N}_2 + \text{H}_2\text{O}$ ) System

Consider the pressure–temperature ( $P$ – $T$ ) diagram of [Figure 4.2a](#), shown schematically for the methane + water system or the nitrogen + water system at conditions above and below the hydrate region. Since methane is the major component of natural gas, this diagram and the associated  $T$ – $x$  diagram (Section 4.1.5) provide phase behavior understanding in the hydrate region for gas systems without a liquid hydrocarbon phase.

The structure of all such phase diagrams rests on experimental data for phase boundaries, and on the Gibbs' Phase Rule discussion of the previous section. The diagrams use symbols of I, L<sub>w</sub>, H, V, and L<sub>HC</sub> to represent ice, liquid water, hydrate, vapor, and liquid hydrocarbon, listed in order of decreasing water contents. By the Gibbs' Phase Rule a two-component system such as methane + water is represented on a pressure–temperature diagram as an area (for two phases), a line (three phases), or a point (four phases). In order to obtain nearly straight lines, in all of Section 4.1 semilogarithmic plots ( $\ln P$  versus  $T$ ) are used.

Consider quadruple point (Q<sub>1</sub>) in Figure 4.2a where four phases (I–L<sub>w</sub>–H–V) coexist. The quadruple point temperature approximates 273 K for all hydrate formers, yet the quadruple pressures vary widely (e.g., 0.0113 MPa for i-C<sub>4</sub>H<sub>10</sub>, 2.56 MPa for CH<sub>4</sub>, and 14.3 MPa for N<sub>2</sub>). Quadruple point (Q<sub>1</sub>) is the starting point for four, three-phase lines:

1. The L<sub>w</sub>–H–V line has pressure–temperature conditions of the most interest in natural gas systems.
2. The I–H–V line, which has a lower  $P$ – $T$  slope than the L<sub>w</sub>–H–V line. Note that there is a data paucity in the region below 273 K, which is avoided industrially (hence a lack of funding) due to problems with ice formation.
3. The I–L<sub>w</sub>–H line rises vertically from the quadruple point, with very large pressure changes for small temperature changes, as typified by incompressible phases.
4. The I–L<sub>w</sub>–V line that connects the quadruple point to the water triple point (I–L<sub>w</sub>–V<sub>w</sub>) (273.16 K, 0.62 kPa), denotes the transition between

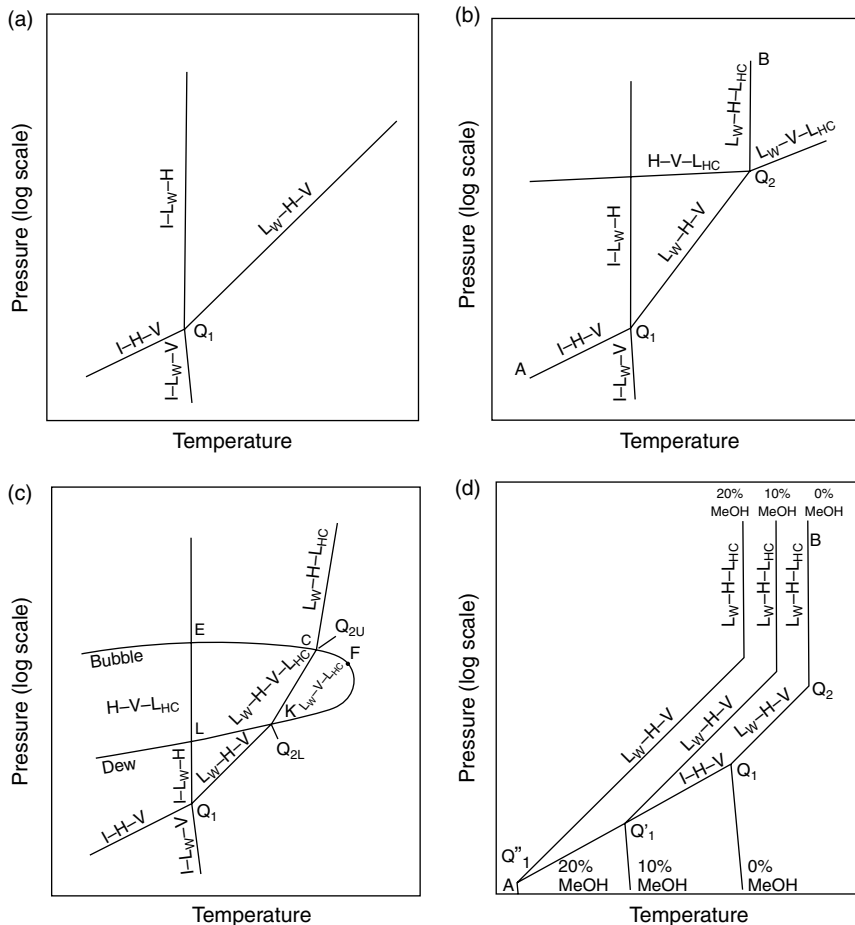


**FIGURE 4.2** Pressure–temperature diagrams. (a) Methane + water or nitrogen + water system in the hydrate region. (b) Hydrocarbon + water systems with upper quadruple points. (c) Multicomponent natural gas + water systems. (d) Hydrocarbon + water systems with upper quadruple points and inhibitors.

water and ice without hydrate formation. Since Q<sub>1</sub> approximates 273 K for all natural gas systems, the I-L<sub>w</sub>-V line extends almost vertically below Q<sub>1</sub> to 0.62 kPa.

In all of Figure 4.2 note that composition, a third dimension, has been compressed onto the two shown (pressure and temperature), so that the lines shown may project from or into the page.

The equation of Table 4.1 from Kamath (1984) enables prediction of the most common regions of interest of simple natural gas components—the pressure and temperature conditions for both L<sub>w</sub>-H-V and I-H-V. When using the equation,

**TABLE 4.2**  
**Natural Gas Component Quadruple Points**

Component	<i>T</i> (K), <i>P</i> (MPa) at <i>Q</i> <sub>1</sub>	<i>T</i> (K), <i>P</i> (MPa) at <i>Q</i> <sub>2</sub>
Methane	272.9, 2.563	No <i>Q</i> <sub>2</sub>
Ethane	273.1, 0.530	287.8, 3.39
Propane	273.1, 0.172	278.8, 0.556
Isobutane	273.1, 0.113	275.0, 0.167
Carbon dioxide	273.1, 1.256	283.0, 4.499
Nitrogen	271.9, 14.338	No <i>Q</i> <sub>2</sub>
Hydrogen sulfide	272.8, 0.093	302.7, 2.239

carefully note the temperature limits. It would be a mistake (for example) to extend the prediction of the L<sub>w</sub>–H–V region beyond the temperature of either quadruple point Q<sub>1</sub> or Q<sub>2</sub> (given in Table 4.2), where those three phases cannot exist.

1. The pressures and temperatures of the L<sub>w</sub>–H–V and the I–H–V lines mark the limits to hydrate formation. At higher temperatures or lower pressures of both lines, hydrate cannot form and the system will contain only aqueous and hydrocarbon fluid phases, while hydrate formation can occur to the left of L<sub>w</sub>–H–V and I–H–V. Since ice and hydrates both cause flow problems, a gas pipeline rule of thumb is to keep the system temperature above the ice point and to the right of the L<sub>w</sub>–H–V and the I–H–V lines, or to displace the L<sub>w</sub>–H–V line below the pipeline operating conditions by injection of a thermodynamic inhibitor such as methanol.
2. The L<sub>w</sub>–H–V line has no upper pressure or temperature limit because the pure methane (or nitrogen) vapor–liquid critical points (at 191 and 126 K respectively) are far below the quadruple point Q<sub>1</sub>. Such low critical temperatures prevent intersection of the vapor pressure line with the L<sub>w</sub>–H–V line above 273 K to produce an upper quadruple point.
3. Similarly, no upper pressure limit to the I–L<sub>w</sub>–H line has been found. Note that these phases are all incompressible, so that a very large pressure change results from only a small temperature change, in a closed system.
4. The areas between the three-phase lines represent the two-phase region held in common with the bounding three-phase lines. For instance, the area between L<sub>w</sub>–H–V and I–H–V is the H–V region in which hydrates are in equilibrium only with vapor (water saturated). Similarly, the L<sub>w</sub>–H two-phase region exists between L<sub>w</sub>–H–V and I–L<sub>w</sub>–H lines, and the I–H two-phase region exists between the I–L<sub>w</sub>–H and I–H–V lines. In this two-dimensional plot the two-phase regions overlap, indicating that the three-phase lines are not all in the plane of the page, but have been compressed into two dimensions, from three, with the third

dimension being composition. The compression of the composition axis onto the  $P-T$  plane causes the two-phase regions to overlap. Two-phase regions are discussed with  $T-x$  diagrams in Section 4.1.5.

- The diagram schematic is the same for simple hydrate systems of sI ( $\text{CH}_4 + \text{H}_2\text{O}$ ) and sII ( $\text{N}_2 + \text{H}_2\text{O}$ ) as well as those of fixed natural gas mixture compositions, without a liquid hydrocarbon phase. Systems containing a liquid hydrocarbon are similar in behavior to the  $\text{C}_3\text{H}_8 + \text{H}_2\text{O}$  diagram, discussed in Section 4.1.2.

It has been shown (Bansal et al., 1993) that curvature in the  $\text{L}_w-\text{H}-\text{V}$  line in [Figure 4.2a](#) results if the guest vapor–liquid critical temperature is slightly below the  $\text{L}_w-\text{H}-\text{V}$  conditions.

#### 4.1.2 Systems (e.g., $\text{H}_2\text{O} + \text{C}_2\text{H}_6$ , $\text{C}_3\text{H}_8$ , or $\text{i-C}_4\text{H}_{10}$ ) with Upper Quadruple Points

[Figure 4.2b](#) shows the equivalent of [Figure 4.2a](#) to be slightly more complex for systems such as ethane + water, propane + water, isobutane + water, or water with the two common noncombustibles, carbon dioxide or hydrogen sulfide. These systems have a three-phase ( $\text{L}_w-\text{V}-\text{L}_{\text{HC}}$ ) line at the upper right in the diagram. This line is very similar to the vapor pressure ( $\text{V}-\text{L}_{\text{HC}}$ ) line of the pure hydrocarbon, because the presence of the almost pure water phase adds a very low vapor pressure (a few mmHg at ambient conditions) to the system.

[Figure 4.2b](#) shows that at the intersection of the  $\text{L}_w-\text{V}-\text{L}_{\text{HC}}$  line with the  $\text{L}_w-\text{H}-\text{V}$  line, a second quadruple point ( $Q_2 = \text{L}_w-\text{H}-\text{V}-\text{L}_{\text{HC}}$ ) is formed. Measured upper quadruple points for simple natural gas components are shown in [Table 4.2](#). Point  $Q_2$  is the origin for two additional three-phase lines: (1) a  $\text{L}_w-\text{H}-\text{L}_{\text{HC}}$  line that is almost vertical due to the three incompressible phases and (2) a  $\text{H}-\text{V}-\text{L}_{\text{HC}}$  line, of less concern, because it exists within the  $\text{L}_w-\text{H}-\text{L}_{\text{HC}}$  and the  $\text{L}_w-\text{H}-\text{V}$  boundaries.

For systems with two quadruple points, the hydrate region is bounded by line  $\text{I}-\text{H}-\text{V}$  at conditions below  $Q_1$ , line  $\text{L}_w-\text{H}-\text{V}$  between  $Q_1$  and  $Q_2$ , as well as line  $\text{L}_w-\text{H}-\text{L}_{\text{HC}}$  at conditions above  $Q_2$ . Hydrates can form at lower temperatures and higher pressures to the left of the region enclosed by the three lines in [Figure 4.2b](#); to the right, no hydrates are possible. Upper quadruple point  $Q_2$  is often approximated as the maximum temperature of hydrate formation, because line  $\text{L}_w-\text{H}-\text{L}_{\text{HC}}$  is almost vertical; however see data in [Chapter 6](#) for exceptions.

In [Figure 4.2b](#), the areas between the three-phase lines represent two-phase regions held in common with the three-phase lines. The area bound by three three-phase lines ( $\text{I}-\text{L}_w-\text{H}$ ,  $\text{L}_w-\text{H}-\text{V}$ , and  $\text{L}_w-\text{H}-\text{L}_{\text{HC}}$ ) is the  $\text{L}_w-\text{H}$  region in which hydrates are in equilibrium only with liquid water. Similarly, the  $\text{H}-\text{V}$  region is between the three three-phase lines ( $\text{H}-\text{V}-\text{L}_{\text{HC}}$ ,  $\text{L}_w-\text{H}-\text{V}$ , and  $\text{I}-\text{H}-\text{V}$ ). Finally, the  $\text{H}-\text{L}_{\text{HC}}$  two-phase region exists between  $\text{L}_w-\text{H}-\text{L}_{\text{HC}}$  and  $\text{H}-\text{V}-\text{L}_{\text{HC}}$  lines and the  $\text{I}-\text{H}$  two-phase region exists between the  $\text{I}-\text{L}_w-\text{H}$  and  $\text{I}-\text{H}-\text{V}$  lines.

See [Section 4.1.5](#) for a  $T-x$  diagram with another perspective of these two-phase regions.

Note that the last paragraph contains two-phase regions (H–V, H–L<sub>HC</sub>, and I–H) for hydrate equilibrium with a phase that is not liquid water. There is a common misconception that hydrates cannot form without a liquid water phase, a condition clearly possible in these diagrams. Professor Kobayashi's laboratory measured hydrate conditions without a free water phase from vapor or liquid systems from 1973 to 2000. Such equilibria are of interest for gas and gas condensate pipelines without a free water phase.

#### 4.1.3 Pressure–Temperature Diagrams for Multicomponent Natural Gas Systems

In [Figure 4.2c](#) for natural gases without a liquid hydrocarbon (or when liquid hydrocarbons exist below 273 K), the lower portion of the pressure–temperature phase diagram is very similar to that shown in Figure 4.2a. Two changes are (1) the L<sub>w</sub>–H–V line would be for a fixed composition mixture of hydrocarbons rather than for pure methane (predictions methods for mixtures are given in Section 4.2 and in [Chapter 5](#)) and (2) quadruple point Q<sub>1</sub> would be at the intersection of the L<sub>w</sub>–H–V line and 273 K, at a pressure lower than that for methane. The other three-phase lines of Figure 4.2a (for I–L<sub>w</sub>–H and I–H–V) have almost the same slope at Q<sub>1</sub>. Otherwise, the same points in Section 4.1.1 apply.

However, for the case in which natural gases contain heavier components, the upper portion of the diagram is more like that shown in Figure 4.2b. A straight line labeled L<sub>w</sub>–H–V represents the hydrate formation region equivalent to the region between quadruple point Q<sub>1</sub> (I–L<sub>w</sub>–H–V) and the upper quadruple point Q<sub>2</sub> (L<sub>w</sub>–H–V–L<sub>HC</sub>) in Figure 4.2b. One significant change in Figure 4.2c is that quadruple point Q<sub>2</sub> becomes a line, as indicated in the next paragraph.

When a liquid hydrocarbon mixture is present, the L<sub>w</sub>–V–L<sub>HC</sub> line in Figure 4.2b broadens to become an area, such as that labeled CFK in Figure 4.2c. This area is caused by the fact that a single hydrocarbon is no longer present, so a combination of hydrocarbon (and water) vapor pressures creates a broader phase equilibrium envelope. Consequently, the upper quadruple point (Q<sub>2</sub>) evolves into a line (KC) for the multicomponent hydrocarbon system.

Line KC may not be straight in the four-phase region but is drawn that way for illustration. The location of the lower point K is determined by the intersection point of the phase envelope ECFKL with the L<sub>w</sub>–H–V line, determined by the methods of Section 4.2 or Chapter 5. To determine the upper point C, first a vapor–liquid equilibrium calculation is performed, assuming the liquid phase (existing the envelope at point C) equals the vapor composition at point K. That liquid is used to calculate a vapor composition which is used in a vapor–liquid water–hydrate calculation to determine the upper intersection with the phase envelope ECFKL. A more thorough treatment of the calculation of multicomponent equilibrium with a condensed hydrocarbon phase is given in Sections 4.3.2.

#### 4.1.4 Pressure–Temperature Diagrams for Systems with Inhibitors

The presence of thermodynamic inhibitors (e.g., salts, alcohols, or glycols) causes a change in the pressure–temperature diagram, as illustrated in Figure 4.2d. For simplicity the diagram only shows the hydrate bounding region (to the left of line AQ<sub>1</sub>Q<sub>2</sub>B) for a pure component system with upper and lower quadruple points (Q<sub>1</sub> and Q<sub>2</sub>). Line AQ<sub>1</sub>Q<sub>2</sub>B in Figure 4.2d is equivalent to line AQ<sub>1</sub>Q<sub>2</sub>B in Figure 4.2b with three slopes that change at the quadruple points.

In Figure 4.2d, the presence of a thermodynamic inhibitor (e.g., methanol) shifts the upper two-thirds of the line Q<sub>1</sub>Q<sub>2</sub>B to the left, approximately parallel (on a semilogarithmic plot of  $\ln P$  versus  $T$ ) to the uninhibited line. With inhibitor, however, the transition temperature from water to ice (Q<sub>1</sub>) is decreased, so that the inhibited L<sub>w</sub>–H–V line intersects the I–H–V at a lower point (labeled Q'<sub>1</sub> for 10 wt% methanol and Q''<sub>1</sub> for 20 wt% methanol). The inhibited three parallel lines represent L<sub>w</sub>–H–V or L<sub>w</sub>–H–L<sub>HC</sub> equilibrium at methanol concentrations (marked 0%, 10%, and 20% MeOH) in the free water phase.

Each line in Figure 4.2d (except for the lower, almost vertical I–L<sub>w</sub>–V lines) bounds hydrate formation conditions listed with a methanol concentration in the free water phase. To the left of each line with “H” in the label, hydrates will form with a water phase of the given methanol composition; to the right of the line hydrates will not form. For example, when the free water phase has 10% methanol, hydrates will not form at pressure–temperature conditions to the right of the line marked 10% MeOH. Yet if no methanol were present, the hydrates would form at pressures and temperatures between the two lines marked 10% and 0% MeOH. Similarly, for process pressure and temperature conditions between the lines marked 10% and 20%, at least 20% methanol in the free water phase would be required to prevent hydrate formation.

For clarity Figure 4.2d has omitted the lines analogous to three three-phase lines in Figure 4.2b (I–L<sub>w</sub>–H that intersects vertically at Q<sub>1</sub> and L<sub>w</sub>–V–L<sub>HC</sub>, and H–V–L<sub>HC</sub> that intersect at Q<sub>2</sub>). Such lines are less important for hydrate formation, but join the diagram at the appropriate, shifted quadruple points. For systems without an upper quadruple point (as in Figure 4.2a) or systems with a liquid hydrocarbon region (as in Figure 4.2c) the hydrate boundary region is similarly shifted to the left of (and approximately parallel to) the uninhibited phase lines.

Other inhibitors such as monoethylene glycol (EG or MEG) and salts shift the hydrate lines similarly, but to a different degree. However, methanol is the most economical inhibitor on a weight basis. Quantitative predictions of inhibitor effects are provided in Sections 4.4 and 5.3.

#### 4.1.5 Temperature–Composition Diagrams for Methane + Water

In the first edition (1989) of this monograph the details of all isobaric temperature–composition ( $T$ – $x$ ) diagrams were discussed, in a synopsis of

Harmens and Sloan (1990). The second edition (1998) simplified those diagrams further. This third edition corrects slight errors in the isobaric  $T$ - $x$  diagram using the work of Huo et al. (2003) and the recent phase diagram simulations of Wierzchowski and Monson (2006). However, much of the value of such diagrams may be obtained from the discussion of a single figure. Consider Figure 4.3, the  $T$ - $x$  diagram and accompanying discussion from Kobayashi and Katz (1949), as slightly corrected by Huo et al. (2003) for  $\text{CH}_4 + \text{H}_2\text{O}$  at a pressure around 48 bar (about 700 psia), just above the critical pressure for methane, but a little lower than normal pipeline pressures.

Figure 4.3 is not drawn to scale. Some regions are expanded and are shown schematically due to the mutual immiscibility of liquid hydrocarbons and water. There are three single phase regions in the diagram: (1) the highest is the single vapor region (V), (2) at the upper left there is the liquid water ( $L_w$ ) single phase

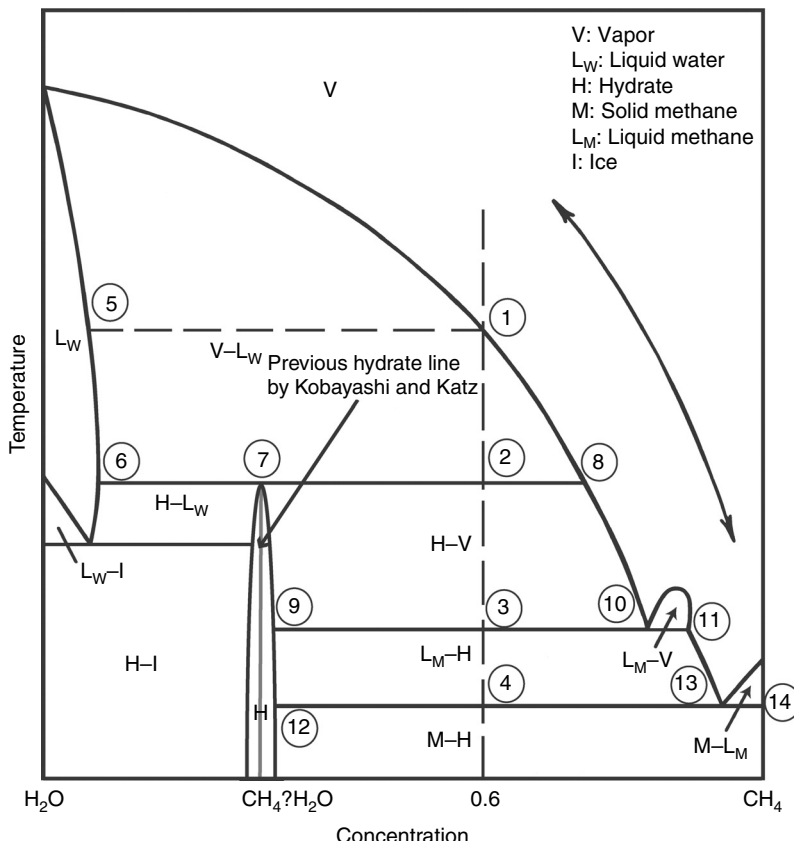


**FIGURE 4.3** Temperature-composition diagrams for methane and water. (Reproduced from Huo, Z., Hester, K., Miller, K.T., Sloan, E.D., *AIChE J.*, **49**, 1300 (2003). With permission from the American Institute of Chemical Engineers.)

region that has less than 0.1 mol% dissolved methane, and (3) the hydrate region that is shown of small variable concentrations straddling the concentration marked  $\text{CH}_4 \cdot ?\text{H}_2\text{O}$ . Each area in [Figure 4.3](#) is marked with the appropriate two-phase equilibrium. Horizontal solid lines represent three-phase equilibrium, all involving the hydrate phase.

To illustrate the phase transitions on a  $T$ - $x$  diagram, consider the cooling of a 60 mol%  $\text{CH}_4 + 40\%$   $\text{H}_2\text{O}$  mixture from a high temperature at a constant pressure in the vapor region, shown as a dashed vertical line. The vapor exists as a single-phase until the water dew point (Point 1) is reached, where the composition of the equilibrium liquid water with a little methane dissolved is Point 5. Further cooling of the gas-liquid mixture causes the amount of the water phase to increase; note that by Gibbs' Phase Rule ( $F = C - P' + 2$ ) two intensive variables (e.g., the  $P$  of the isobaric diagram and  $T$ ) are required to specify each fluid composition at the two-phase borders.

Cooling the system is continued until the temperature of Point 2, where the hydrate phase (vertical area that begins at Point 7) forms from the vapor (Point 8) and liquid (Point 6). At Point 2 three phases ( $\text{L}_w$ - $\text{H}$ - $\text{V}$ ) coexist for two components, so Gibbs' Phase Rule ( $F = 2 - 3 + 2$ ) indicates that only the isobaric pressure of the entire diagram is necessary to obtain the temperature and the concentrations of the three phases ( $\text{L}_w$ ,  $\text{H}$ , and  $\text{V}$ ) in equilibrium.

At the three-phase condition, the calculated methane mole fractions in the aqueous, sI hydrate, and vapor phases are 0.0014 (Point 6), 0.14 (Point 7), and 0.9997 (Point 8) respectively, illustrating that the aqueous and vapor concentrations shown in [Figure 4.3](#) are expanded for illustration purposes. Note that the isobaric three-phase temperature at Point 2 marks one  $P$ - $T$  condition on the three-phase line ( $\text{L}_w$ - $\text{H}$ - $\text{V}$ ) shown in [Figure 4.2a](#), with prediction methods in [Table 4.1](#) and [Section 4.2](#). In both Figures 4.2a and 4.3, at temperatures above this line, hydrates cannot form at the specified pressure.

Further heat removal at constant temperature will result in the complete conversion of the free water phase to hydrate at the same initial overall composition of 60% methane. The system enters the two-phase hydrate-vapor ( $\text{H}$ - $\text{V}$ ) region just below the horizontal line at Point 2. By specifying the water composition of the vapor in the two-phase ( $\text{H}$ - $\text{V}$ ) region (along the negatively sloping line between Points 8 and 10), the gas processor determines how dry the gas must be to prevent the possibility of hydrate formation. The position of the vapor composition line determines, for example, whether a glycol drying column or a molecular sieve dessicant should be used to dehydrate the gas.

At still lower temperatures of the original mixture, some of the vapor condenses to liquid methane at the three-phase ( $\text{H}$ - $\text{V}$ - $\text{L}_M$ ) boundary (Point 3). Again the three-phase temperature and phase compositions (Points 9, 10, and 11) are specified by the single variable of pressure ( $F = C - P' + 2 = 2 - 3 + 2$ ). Below this three-phase line the vapor phase is totally condensed to a liquid resulting in a two-phase ( $\text{H}$ - $\text{L}_M$ ) region between Points 3 and 4.

Point 4 is at the temperature of the lowest three-phase line ( $\text{H}$ - $\text{L}_M$ - $\text{M}$ ), which occurs just below the solidification point of pure methane ( $\text{M}$ ). Below this line

(connecting Points 12, 4, 13, and 14) the liquid methane phase disappears and hydrate exists only with solid methane.

A comprehension of Figure 4.3 has value because a similar phase diagram could be drawn for a natural gas of fixed composition between the quadruple points ( $Q_1$  and  $Q_{2L}$ ). The same phase transitions and boundaries would qualitatively occur, with the artificial constraint that all hydrocarbon phases be of the same composition as the original gas. A second useful outcome of binary phase diagrams like Figure 4.3 is the use of the lever rule (Koretsky, 2004, p. 367) at constant temperature to determine relative phase amounts; note that the lever rule can be applied for quantitatively correct phase diagrams.

#### 4.1.6 Solubility of Gases Near Hydrate Formation Conditions

The solubility of hydrocarbons in the aqueous phase determines the width of the region  $L_w$  marked on the  $T-x$  diagram of Figure 4.3. Section 3.1.1.2 provides numerical values of atmospheric solubilities, enthalpies, and entropies of solution. The solubility phenomena is that water molecules form networks with short-lived, partial hydrogen-bonded clusters around solute molecules, giving solubility maxima for molecules with hydrate guest diameters. In Section 3.1.2.1 it was suggested that clustering is related to hydrate metastability and nucleation.

There are only few data sets of aqueous solubility for systems with hydrates: (1) methane and ethane solubility in water as a function of temperature ramping rate (Song et al. 1997), (2) carbon dioxide solubility in water by Yamane and Aya (1995), (3) methane in water and in seawater (Besnard et al., 1997), (4) methane in water in  $L_w-H$  region [see Servio and Englezos (2002) and Chou and Burruss, Personal Communication, December 18, 2006, Chapter 6]. As a standard for comparison, Handa's (1990) calculations for aqueous methane solubility are reported in Table 4.3.

While Table 4.3 shows solubility both above and below the hydrate point, at the three-phase hydrate condition Handa's predictions show a sharp maximum in solubility with pressure at constant temperature. In Holder's laboratory, Toplak (1989) measured the solubility of gas in liquid water around the hydrate point, both in water that had formed hydrates and in water with no residual structure; his results show no dramatic change in pure component solubility at the three-phase ( $L_w-H-V$ ) condition. Kobayashi and coworkers (Besnard et al., 1997) measured a significant solubility increase at the hydrate point beyond that calculated using Henry's law. However, comprehensive solubility measurements around the hydrate point await further experiments.

#### 4.1.7 Pressure–Temperature Diagrams for Structure H Systems

The pressure–temperature diagram for structure H has both similarities and differences from those diagrams shown above. Because the new hydrate was discovered

**TABLE 4.3**  
**Calculations of Methane Solubility in Water and Seawater,  
at Conditions Above and Below the Hydrate Point**

Temperature = 273.15 K			Temperature = 278.15 K		
P (bar)	Water $10^3 x_{\text{CH}_4}$	Seawater $10^3 x_{\text{CH}_4}$	P (bar)	Water $10^3 x_{\text{CH}_4}$	Seawater $10^3 x_{\text{CH}_4}$
1	0.04667	0.03587	1	0.04022	0.03133
26.29 <sup>a</sup>	1.113	NA	42.73 <sup>a</sup>	1.473	NA
28.95 <sup>b</sup>	NA	0.9334	49.54 <sup>b</sup>	NA	1.297
50	1.931	1.484	100	2.801	2.182
100	3.194	2.455	150	3.555	2.769
150	4.024	3.093	200	4.105	3.198
200	4.619	3.550	250	4.544	3.539
250	5.095	3.916	300	4.926	3.836
300	5.506	4.232	350	5.267	4.102
350	5.879	4.519	400	5.582	4.347
400	6.222	4.783	450	5.875	4.576
450	6.545	5.031	500	6.153	4.793
500	6.849	5.264			

<sup>a</sup> Three-phase hydrate formation pressure in water.

<sup>b</sup> Three-phase hydrate formation pressure in seawater.

*Source:* From Handa, Y.P., *J. Phys. Chem.*, **94**, 2652, 1990. With permission.

in 1987, few data have been determined and thus limit the discussion. For the most comprehensive treatment, the reader is referred to the thesis of Mehta (1996).

A phase diagram for xenon + neo-hexane is presented in Figure 4.4, because the best measurements are available for this system (Makogon et al., 1996). While xenon is not a component of natural gas (or condensate), and because the xenon diameter is only 0.2 Å larger than CH<sub>4</sub>, the phase diagram for CH<sub>4</sub> + neo-hexane is similar, but at higher pressures. The schematic of Figure 4.4 is very similar for many structure H systems in natural gas and for hydrocarbon processing.

The following points should be noted regarding the structure H phase diagram shown in Figure 4.4:

1. The temperatures and pressures for the sH system are very similar to those found in sI and sII diagrams. If a hydrate forms in a pipeline with both gas and condensate/oil phases present, examining the pressure–temperature conditions may be insufficient to determine the hydrate crystal structure.
2. Two quintuple points (Q<sub>1</sub> and Q<sub>2</sub>) fix the positions of the lines in Figure 4.4. Each point (Q<sub>1</sub> and Q<sub>2</sub>) is the origin of five four-phase lines. However, only the two lines of central importance (discussed below) have been measured from each quintuple point.

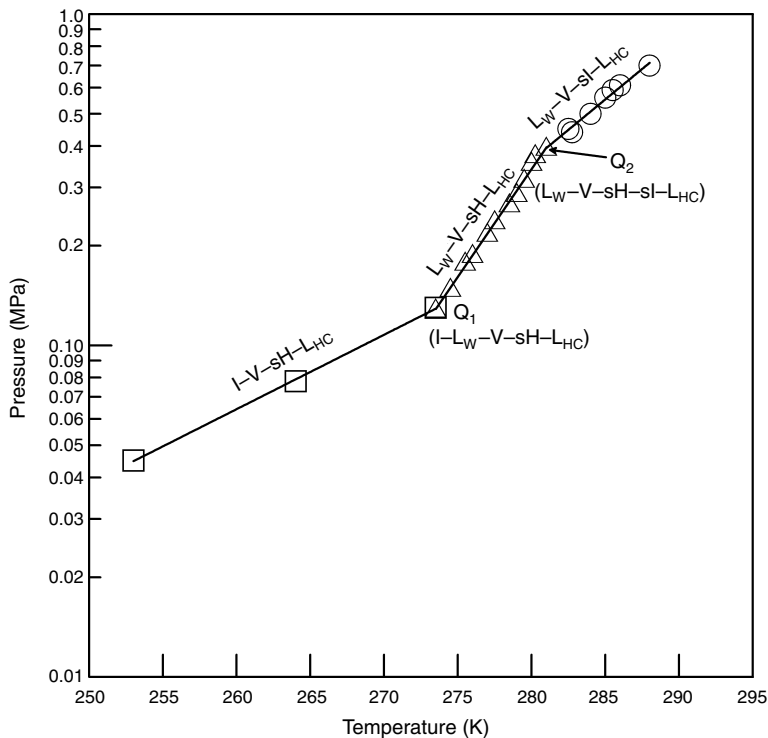


**FIGURE 4.4** Pressure–temperature diagram for Xenon + Neo-hexane. (Reproduced from Makogon T.Y., Mehta, A.P., Sloan, E.D., *J. Chem. Eng. Data*, **41**, 315 (1996). With permission from the American Chemical Society.)

3. Structure H has only four-phase equilibrium lines (as opposed to the three-phase lines in Figure 4.2). Four-phase lines are required by Gibbs' Phase Rule, because a minimum of three components (a large and small guest, and water) are present. Structure H can only form with two guests (minimum)—one in both small cavities ( $5^{12}$  and  $4^35^66^3$ ) and one in the large ( $5^{12}6^8$ ) cavity; water must also be present. The large hydrate component is usually present as a liquid with a low vapor pressure. In unusual cases (e.g., adamantane) the large guest component may be present in the system as a solid.
4. The lower quintuple point ( $Q_1$ ) is the location of five coexisting phases—namely,  $I-L_w-sH-V-L_{HC}$ . The position of  $Q_1$  is determined by the intersection of the  $I-sH-V-L_{HC}$  line and the  $L_w-sH-V-L_{HC}$  line, close to the ice point temperature (273.15 K). However, the pressure of  $Q_1$  is a function of the hydrate guests.
5. The upper quintuple point ( $Q_2$ ) has a common line with  $Q_1$  ( $L_w-sH-V-L_{HC}$ ), but it also is the origin of a new line ( $L_w-sI-V-L_{HC}$ ). At temperatures higher than  $Q_2$  the hydrate phase is sI rather than sH.

Therefore Q<sub>2</sub> places an upper temperature limit on sH, while allowing for sI hydrate equilibrium at higher temperatures.

With the above beginning, much remains to be done with such a phase diagram, and this is an area of active research. Ripmeester and Ratcliffe (1991) noted that because structure H systems form with many hydrocarbon systems, there is the chance it may dominate as a hydrate type. Mehta and Sloan (1996a) discuss cases in which structure H forms in preference to sII in condensate systems. However, measurements by Tohidi et al. (2001), and Mehta and Ripmeester (2002) suggested that for most reservoir fluids, sII would be the common hydrate with sH as the exception. It should be noted that early workers (Becke et al., 1992) were surprised to find sH while investigating a liquid hydrocarbon system of interest to North Sea operations. On the strength of gas compositions Sassen and MacDonald (1994) and Pohlman et al. (2005) reason that sH hydrates were found in the Gulf of Mexico and the Cascadia Margin, respectively.

## 4.2 THREE-PHASE (L<sub>W</sub>-H-V) EQUILIBRIUM CALCULATIONS

The conditions of three-phase (L<sub>W</sub>-H-V) equilibrium are the most useful. In particular, methods to calculate the temperature and pressure at which hydrates form from a given gas composition and free water have both industrial and academic applications.

There are comparatively few measurements of the hydrate phase composition, due to experimental difficulty. Hydrate phase difficulties arise because water is often occluded in the hydrate mass, separation of hydrate and water is difficult, and the hydrate phase of mixtures is often inhomogeneous in experiments. Consequently, the ratio of water to hydrocarbon is often inaccurate. As discussed in [Chapter 6](#), only over the last two decades have experimental techniques (e.g., diffraction and NMR and Raman spectroscopy) become accurate enough to determine the degree of filling of hydrate cavities with different types of molecules.

In this section two prediction techniques are discussed, namely, the gas gravity method and the  $K_{vsi}$  method. While both techniques enable the user to determine the pressure and temperature of hydrate formation from a gas, only the  $K_{vsi}$  method allows the hydrate composition calculation. Calculations via the statistical thermodynamics method combined with Gibbs energy minimization ([Chapter 5](#)) provide access to the hydrate composition and other hydrate properties, such as the fraction of each cavity filled by various molecule types and the phase amounts.

Because the two prediction techniques of this chapter were determined over half a century ago, they apply only to sI and sII hydrates, without consideration of the more recent sH, which always contains a heavier component. For structure H equilibrium, only the statistical thermodynamics method of Chapter 5 is available for prediction of hydrate pressure, temperature, and composition.

The two calculation techniques in this chapter may be regarded as successive approximations to hydrate phase equilibrium, increasing both in accuracy and in

sophistication. The first method, in Section 4.2.1, based upon the parameter of gas gravity, is a simple graphical technique that provides a first-order accuracy estimate of hydrate formation. The second prediction technique of Section 4.2.2, the  $K_{vsi}$ -value method, is both more accurate and slightly more complex than the gravity method. Both methods are suitable for hand calculation.

A third technique is based upon the statistical thermodynamics approach of van der Waals and Platteeuw (1959a) and provides the best approximation to hydrate phase equilibrium. It has the additional advantage of being extendable to all phase equilibrium regions discussed above. Unfortunately, this third method is too lengthy for inclusion in this chapter without disruption of presented concepts. The discussion of the third method is deferred until [Chapter 5](#); a CSMGem computer program and User's Manual on the CD with this book provides access; the Appendix has a User's Guide—with examples of this program.

#### 4.2.1 The Gas Gravity Method

The simplest method of determining the temperature and pressure of a gas mixture three-phase (L<sub>w</sub>–H–V) conditions is available through the gas gravity charts of Katz (1945). Gas gravity is defined as the molecular mass of the gas divided by that of air. In order to use this chart, reproduced as Figure 4.5 from [Figure 1.4](#),

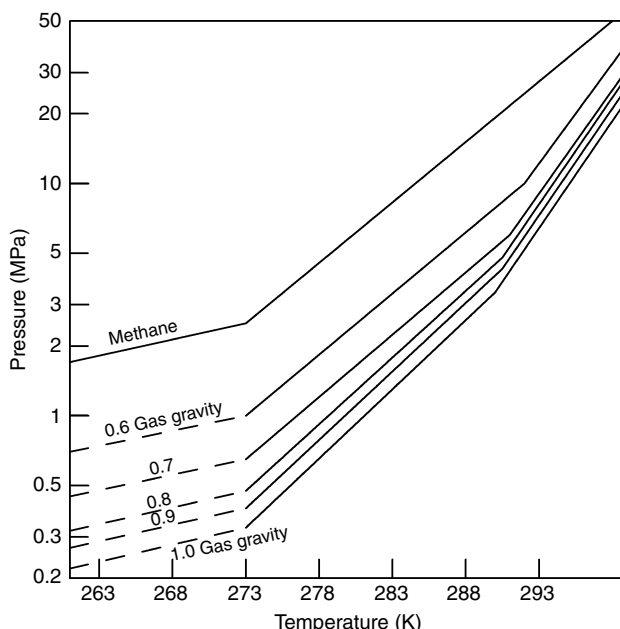


**FIGURE 4.5** Gas gravity chart for prediction of three-phase (L<sub>w</sub>–H–V) pressure and temperature. (Reproduced from Katz, D.L., *Trans. AIME*, **160**, 140 (1945). With permission from the American Institute of Mining, Metallurgical, and Petroleum Engineers.)

the gas gravity is calculated and either temperature or pressure is specified. The second intensive variable (either pressure or temperature) at which hydrates will form is read directly from the chart. The following example from the original work by Katz illustrates chart use.

### Example 4.2: Calculating Hydrate Formation Using Gas Gravity Chart

Find the pressure at which a gas composed of 92.67 mol% methane, 5.29% ethane, 1.38% propane, 0.182% i-butane, 0.338% n-butane, and 0.14% pentane form hydrates from free water at a temperature of 283.2 K (50°F).

#### *Solution*

The gas gravity is calculated as 0.603 by the procedure below:

Component	Mol fraction $y_i$	Mol wt MW	Avg mol wt in mix $y_i \cdot MW$
Methane	0.9267	16.043	14.867
Ethane	0.0529	30.070	1.591
Propane	0.0138	44.097	0.609
i-Butane	0.00182	58.124	0.106
n-Butane	0.00338	58.124	0.196
Pentane	0.0014	72.151	0.101
	1.000		17.470

$$\text{Gas Gravity} = \frac{\text{MW of Gas}}{\text{MW of Air}} = \frac{17.470}{28.966} = 0.603$$

At 283.2 K, the hydrate pressure is read as 3.1 MPa.

Similarly Example 4.1 used the gas gravity method to predict hydrate pressure of 1.95 MPa at 278.2 K for a mixture of 95.6% CH<sub>4</sub> + 4.4% C<sub>3</sub>H<sub>8</sub> as compared to the experimental value of 1.3 MPa.

The purpose of the original chart was to enable the determination of the hydrate limits to adiabatic expansion of a gas, as detailed in Section 4.2.1.1. The hydrate formation lines on Figure 4.5 appear to be fairly linear at low temperatures with a slope change above 288 K for each gravity; this slope change is intentional and has been ascribed to a change in hydrate structure (Katz, D.L., Personal Communication, November 14, 1983).

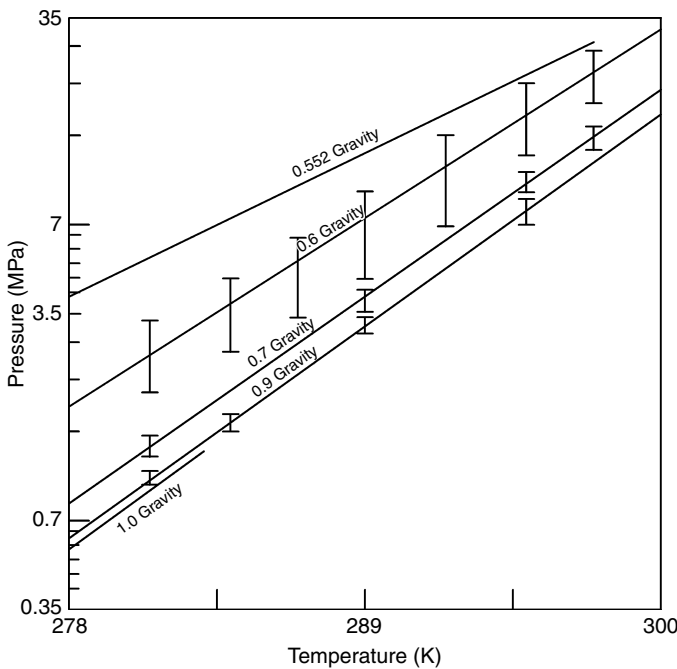


**FIGURE 4.6** Gas gravity chart error bars. (Reproduced from Sloan, E.D., in *Proc. 63rd Annual Convention of Gas Processors Association*, **63**, 163 (1984). With permission from the Gas Processors Association.)

All of the qualitative trends shown in Figure 4.5 are correct and thus provide a valuable heuristic as a check for more sophisticated calculations. For example, the figure correctly indicates a logarithmic pressure increase with temperature over a short range. Over a wider temperature range the logarithmic pressure is more nearly linear with reciprocal absolute temperature. The figure also correctly shows that gases with heavier components cause hydrates to form at lower pressures for a given temperature (or at higher temperatures for a given pressure).

The gas gravity method to predict hydrate formation was generated from a limited amount of data as well as with calculations performed (and therefore the accuracy determined) via the  $K_{vsi}$ -value method of Section 4.2.2. Typical calculated error bars (Sloan, 1984) for the gas gravity chart are presented in Figure 4.6, compared against the statistical thermodynamic approach of Chapter 5. The original chart of Figure 4.5 was generated for gas containing only hydrocarbons, and so should be used with caution for those gases with substantial amounts of non-combustibles (i.e., CO<sub>2</sub>, H<sub>2</sub>S, N<sub>2</sub>). While this method is very simple, it should be considered as approximate. In approximately 60 years since its conception, more hydrate data and prediction methods have caused the gravity method to be used as a first estimate, whose principal asset is ease of calculation.

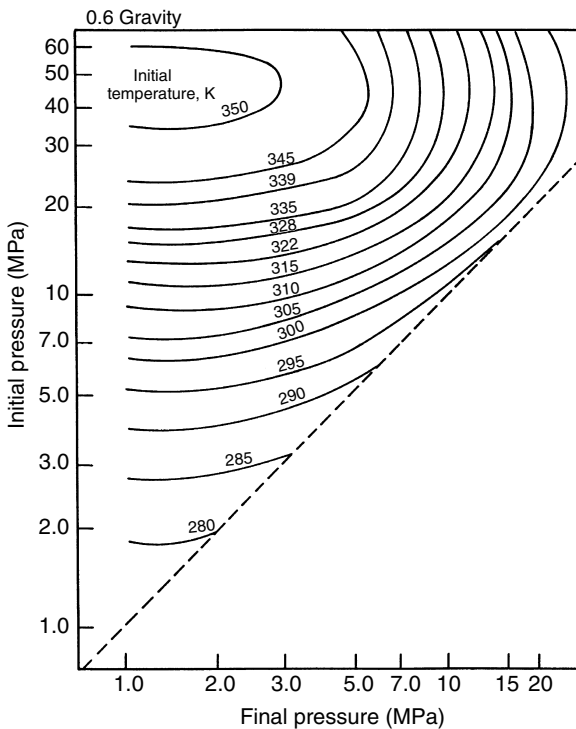


**FIGURE 4.7** Joule–Thomson limits to 0.6 gravity gas expansion. (Reproduced from Katz, D.L., *Trans. AIME*, **160**, 140 (1945). With permission from the American Institute from Mining, Metallurgical, and Petroleum Engineers.)

#### 4.2.1.1 Hydrate limits to gas expansion through a valve

The generation of the hydrate Joule–Thomson charts, such as Figure 4.7, for hydrate formation limits to gas adiabatic expansion was the original goal for construction of the hydrate gas gravity chart in Figure 4.5. A series of “expansion limits” or Joule–Thomson charts for gas gravities between 0.55 and 1.0 are available in the original article by Katz (1945). Figures 4.7 through 4.9 (for gas gravities of 0.6, 0.7, and 0.8, respectively) are presented as those of the highest utility. These Joule–Thomson charts were generated using the initial Mollier (enthalpy–entropy) charts for natural gas by Brown (1945), without accounting for the expansion of any free water present before the valve—assuming a single-phase expansion of natural gas, to the initiation limit of hydrates.

The pressure and temperature of the gas normally decreases upon expansion along an isenthalpic curve ( $\Delta H = 0$ ) until the intersection with the hydrate boundary of Figure 4.5 is encountered, which provided one point on a figure such as Figure 4.7. Multiple points were calculated to construct each figure. The charts enabled the user to estimate the limits to adiabatic expansion before

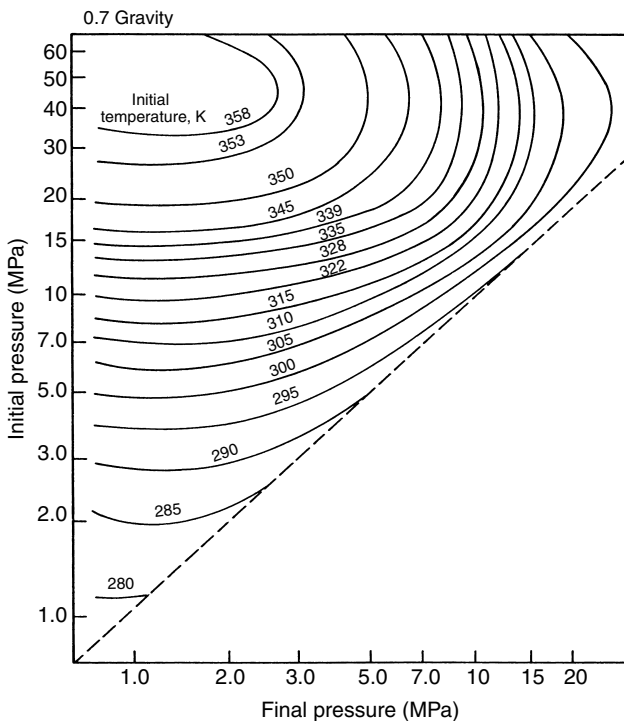


**FIGURE 4.8** Joule–Thomson limits to 0.7 gravity gas expansion. (Reproduced from Katz, D.L., *Trans. AIME*, **160**, 140 (1945). With permission from the American Institute of Mining, Metallurgical, and Petroleum Engineers.)

hydrate formation occurred. The examples given below, of the use of Figure 4.7, were also taken from the original work by Katz (1945).

### Example 4.3: Calculations of Hydrate Formation on Gas Expansion

1. To what pressure may a 0.6 gravity gas at 13.8 MPa (2000 psia) and 311 K (100°F) be expanded without danger of hydrate formation?

*Solution*

From Figure 4.7 read 7.24 MPa (1050 psia).

2. A 0.6 gravity gas is to be expanded from 10.34 MPa (1500 psia) to 3.45 MPa (500 psia). What is the minimum initial temperature that will permit the expansion without danger of hydrates?

*Solution*

From Figure 4.7 the answer is read as 310 K (99°F) or above.

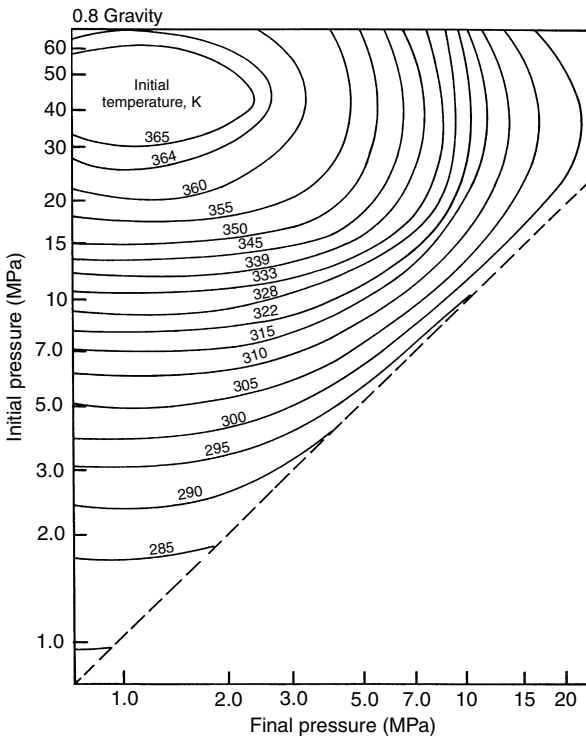


**FIGURE 4.9** Joule–Thomson limits to 0.8 gravity gas expansion. (Reproduced from Katz, D.L., *Trans. AIME*, **160**, 140 (1945). With permission from the American Institute of Mining, Metallurgical, and Petroleum Engineers.)

Figures 4.7 through 4.9 are provided for hydrate limits to isenthalpic Joule–Thomson expansions, such as that which occurs when a gas with entrained free water droplets flows through a valve. A similar set of charts could in principle be determined for hydrate limits to isentropic ( $\Delta S = 0$ ) expansions such as would occur when a gas flows through a perfect turboexpander of a modern gas processing plant. To date, however, no such charts have been generated.

The inaccuracies listed in the previous section for the gas gravity chart are inherent in the expansion charts of Figures 4.7 through 4.9 due to their method of derivation. Accuracy limits to these expansion curves have been determined by Loh et al. (1983) who found, for example, that the allowable 0.6 gravity gas expansion from 339 K and 24 MPa was 2.8 MPa rather than the value of 4.8 MPa, given in Figure 4.7.

The work of Loh et al. (1983) was done using the same principles as those used to generate Figure 4.7. That is, from the initial temperature and pressure, an isenthalpic cooling curve, and its intersection with the hydrate three-phase locus, was determined. However, the isenthalpic line was determined via the Soave–Redlich–Kwong equation-of-state rather than the Mollier charts of

Brown, and the statistical thermodynamic method of van der Waals and Platteeuw (1959a) was substituted for the three-phase hydrate line prediction by the gas gravity chart of Katz.

#### 4.2.2 The Distribution Coefficient ( $K_{vsi}$ -Value) Method

The distribution coefficient method, often called the “ $K_{vsi}$ -value” method, was conceived by Wilcox et al. (1941) and finalized by Carson and Katz (1942). The best methane, ethane, and propane charts are from the latter reference. Updated charts are presented for carbon dioxide (Unruh and Katz, 1949), hydrogen sulfide (Noaker and Katz, 1954), nitrogen (Jhaveri and Robinson, 1965), isobutane (Wu et al., 1976), and n-butane (Poettmann, 1984), as well as for a method that is a function of hydrate structure (Mann et al., 1989).

Carson and Katz noted that their experimental hydrate composition changed at different temperatures and pressures in a manner indicative of a solid solution of mixtures, rather than segregated macroscopic quantities of pure hydrocarbons within the hydrate. The concept of a solid solution enabled the notion of the mole fraction of a guest component in the solid phase hydrate mixture, on a water-free basis. Carson and Katz defined a vapor–solid distribution coefficient ( $K_{vsi}$ ) for each component as

$$K_{vsi} \equiv y_i/x_{si} \quad (4.1)$$

where

$y_i$  = mole fraction of component  $i$  in the water-free vapor and

$x_{si}$  = mole fraction of component  $i$  in the water-free, solid hydrate.

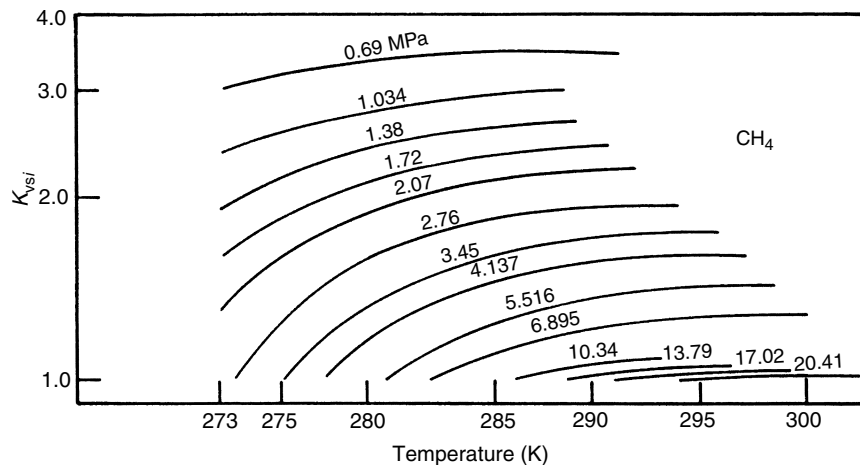
The  $K_{vsi}$  values for natural gas components are presented as a function of temperature and pressure in Figures 4.10 through 4.17. By viewing these charts one may quantitatively determine in which phase a component will concentrate. For example, components such as methane and nitrogen have  $K_{vsi}$  values always greater than unity, so they concentrate in the vapor rather than the hydrate; components such as propane or isobutane with  $K_{vsi}$  values normally less than unity are concentrated in the hydrate phase. Equation 4.2 was used to fit all of the  $K_{vsi}$  values in Figures 4.10 through 4.17.

$$\begin{aligned} \ln K_{vsi} = & A + B^*T + C^*\Pi + D^*T^{-1} + E^*\Pi^{-1} + F^*\Pi^*T + G^*T^2 + H^*\Pi^2 \\ & + I^*\Pi^*T^{-1} + J^*\ln(\Pi^*T^{-1}) + K^*(\Pi^{-2}) + L^*T^*\Pi^{-1} + M^*T^{2*}\Pi^{-1} \\ & + N^*\Pi^*T^{-2} + O^*T^*\Pi^{-3} + Q^*T^3 + R^*\Pi^{3*}T^{-2} + S^*T^4 \end{aligned} \quad (4.2)$$

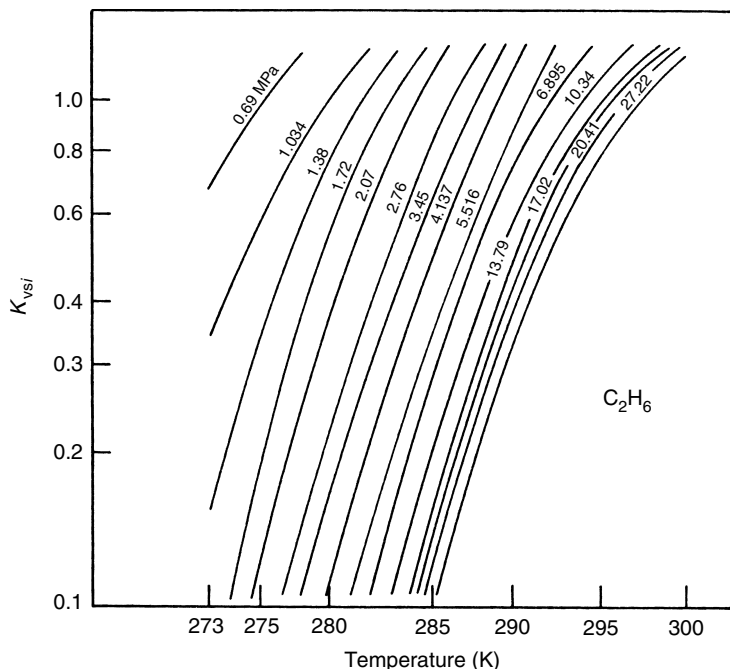
where

$\Pi$  = pressure (psia) and

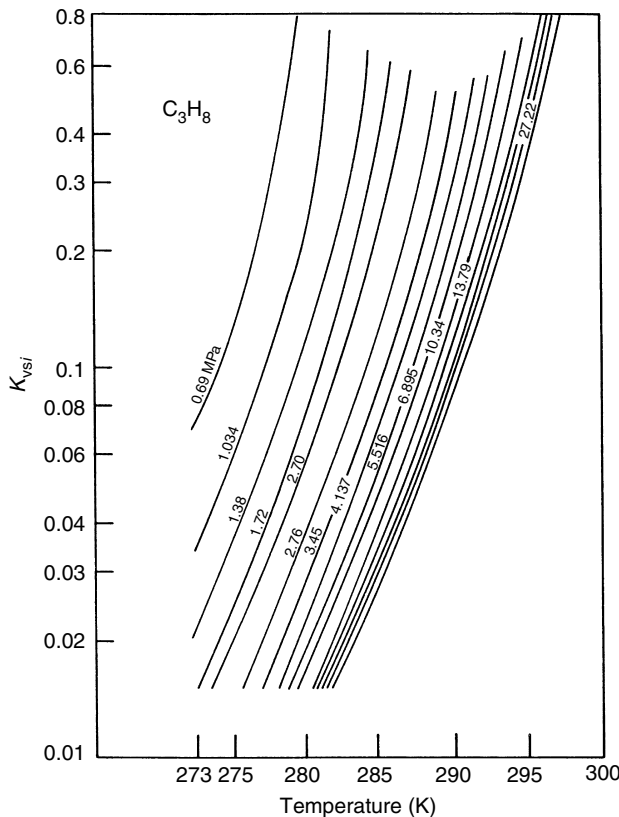
$T$  = temperature ( $^{\circ}$ F).



**FIGURE 4.10** Methane  $K_{vsi}$  chart. (Reproduced from Carson, D.B., Katz, D.L., *Trans. AIME*, **146**, 150 (1942). With permission from the American Institute of Mining, Metallurgical, and Petroleum Engineers.)



**FIGURE 4.11** Ethane  $K_{vsi}$  chart. (Reproduced from Carson, D.B., Katz, D.L., *Trans. AIME*, **146**, 150 (1942). With permission from the American Institute of Mining, Metallurgical, and Petroleum Engineers.)



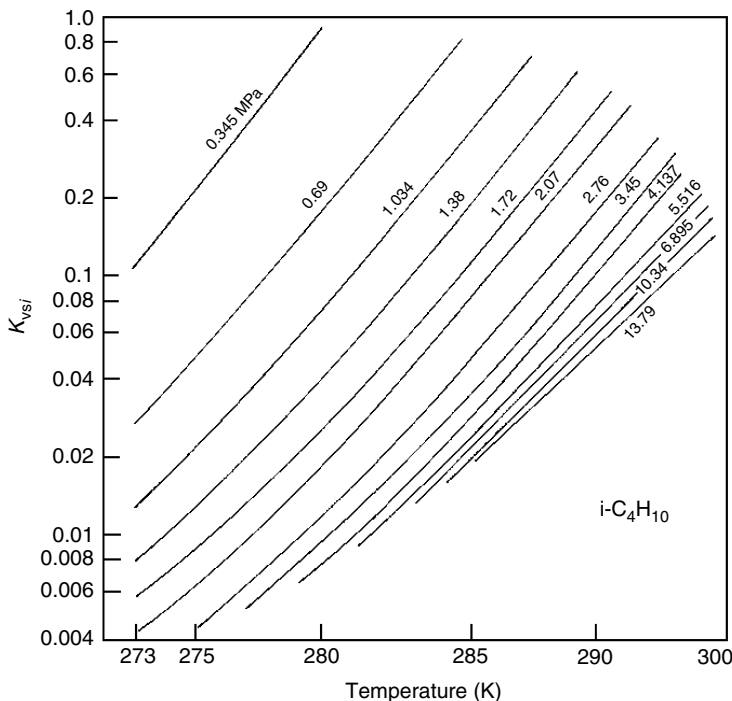
**FIGURE 4.12** Propane  $K_{vsi}$  chart. (Reproduced from Carson, D.B., Katz, D.L., *Trans. AIME*, **146**, 150 (1942). With permission from the American Institute of Mining, Metallurgical, and Petroleum Engineers.)

Table 4.4a presents the parameters of Equation 4.2, with an indication of the correlation coefficient. The  $K_{vsi}$ -value charts or equations are used to determine the temperature or pressure of three-phase (Lw-H-V) hydrate formation. The condition for initial hydrate formation from free water and gas is calculated from an equation analogous to the dew point in vapor-liquid equilibrium, at the following condition:

$$\sum_{i=1}^n \frac{y_i}{K_{vsi}} = 1.0 \quad (4.3)$$

which is the requirement that the nonaqueous hydrate mole fractions sum to unity.

At the three-phase pressure for a given temperature and gas phase composition, the sum of the mole fraction of each component in the vapor phase divided by the  $K_{vsi}$  value of that component must equal unity. In order to have hydrates



**FIGURE 4.13** Isobutane  $K_{vsi}$  chart. (Reproduced from Wu, B.-J., Robinson, D.B., Ng, H.-J., *J. Chem. Thermodyn.*, **8**, 461 (1976). With permission from Academic Press, Ltd.)

present with a gas mixture, it is always necessary to have at least one  $K_{vsi}$  value greater than unity and at least one  $K_{vsi}$  value less than unity. Using interpolation and extrapolation, the pressure is changed in an iterative manner, and other  $K_{vsi}$  values are determined until the above sum ( $\sum y_i/K_{vsi}$ ) equals one at the point of hydrate formation (or dissociation). A similar technique is followed to determine the three-phase temperature at a given pressure. The technique is illustrated with the following example from Carson and Katz (1942) for the calculation of the pressure for hydrate formation.

#### Example 4.4: Calculating Hydrate Formation Using $K_{vsi}$ Method

Determine the pressure of hydrate formation at 283.2 K (50°F) from a gas with a composition of 78.4 mol%  $\text{CH}_4$ , 6.0%  $\text{C}_2\text{H}_6$ , 3.6%  $\text{C}_3\text{H}_8$ , 0.5%  $i\text{-C}_4\text{H}_{10}$ , 1.9%  $n\text{-C}_4\text{H}_{10}$ , 9.4%  $\text{N}_2$ , 0.2%  $\text{CO}_2$ .

*Solution:*

Guess two pressures (300 and 350 psia) as approximations to the condition at which  $\sum y_i/K_{vsi} = 1.0$ . Read the corresponding value of  $K_{vsi}$  for each

component at those pressures, to use in the table given below:

Component	$y_i$ , Mole fraction	$K_{vsi}$ at	$K_{vsi}$ at	
		2.07 MPa (300 psia)	$y_i/K_{vsi}$	2.41 MPa (350 psia)
Methane	0.784	2.04	0.384	1.90
Ethane	0.060	0.79	0.076	0.63
Propane	0.036	0.113	0.318	0.09
i-Butane	0.005	0.046	0.108	0.034
n-Butane	0.019	$\infty$	0.0	$\infty$
Nitrogen	0.094	$\infty$	0.0	$\infty$
Carbon dioxide	0.002	3.0	0.0007	2.3
Sum	1.000		0.8874	1.0553

Since the value of  $\Sigma y_i/K_{vsi}$  is below unity at 300 psia, but above unity at 350 psia, the pressure at  $\Sigma y_i/K_{vsi} = 1.0$  must lie between 300 and 350 psia. Interpolating linearly, the chart values yield  $\Sigma y_i/K_{vsi} = 1.0$  at 2.3 MPa (333 psia). The experimental value of hydrate formation at 283.2 K (50°F) is 2.24 MPa (325 psia).

Similarly, in Example 4.1, the hydrate pressure for 95.6% CH<sub>4</sub> + 4.4% C<sub>3</sub>H<sub>8</sub> was calculated as 1.26 MPa with an experimental value of 1.3 MPa.

---

Müller-Bongartz (Personal Communication, February 6, 1989) tested the accuracy of predictions from Equation 4.2 against the ternary and multicomponent data in Chapter 6 with the results given in Table 4.4b. From these comparisons, it can be seen that the polynomial fit of Equation 4.2 is not entirely satisfactory, but it will often serve as an acceptable estimate, which may be refined through use of Figures 4.10 through 4.17, or via the method given in Chapter 5, with the User's Examples in the Appendix.

The accuracy of the  $K_{vsi}$ -value method is impressive, considering the fact that the method preceded the knowledge of the crystal structure. Carson and Katz (1942) labeled their charts as tentative, yet the original methane, ethane, and propane charts continue to be useful. The  $K_{vsi}$  chart of methane was constructed from three data points at 4.14 MPa (600 psia), while the curves at other pressures were based on two data points and drawn symmetrically to the curve at 4.14 MPa (Katz, D.L. Personal Communication, November 14, 1983).

The  $K_{vsi}$  charts for components other than methane were derived from binary experimental data, with the  $K_{vsi}$  values for the second component based on that for methane. That is, at an experimental hydrate formation temperature, pressure, and binary gas composition, the values of  $y_i$  were fixed and the methane value of

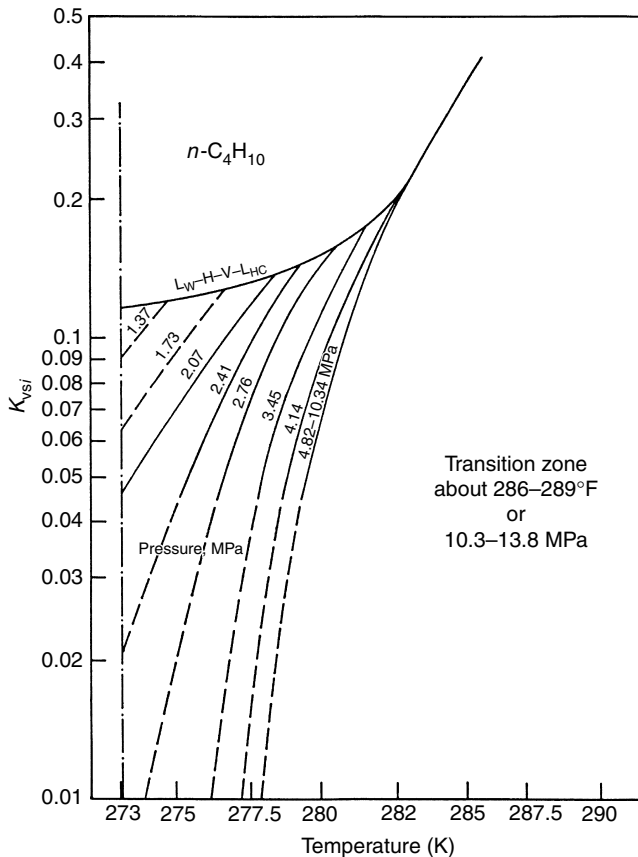


**FIGURE 4.14** n-Butane  $K_{vsi}$  chart. (Reproduced from Poettmann, F.H., *Hydrocarbon Proc.*, **63**, 111 (1984). With permission from Gulf Publishing Co.)

$K_{vsi}$  was found on the original methane chart. Then the only unknown, the  $K_{vsi}$  value of the second component was calculated, which satisfied Equation 4.3. With this calculation method one might expect  $K_{vsi}$  charts for other components to be less accurate than that for methane, because any inaccuracy in the methane chart is incorporated in succeeding charts.

In the discussion appendix of the original paper by Carson and Katz (1942), Hammerschmidt indicated that, while the method was acceptable for gases of “normal” natural gas composition, an unacceptable deviation was obtained for a gas rich in ethane, propane, and the butanes. More work is also required to revise the  $K_{vsi}$ -value charts for two components, namely, carbon dioxide and nitrogen. In three-phase hydrate data for binary mixtures of carbon dioxide and propane, Robinson and Mehta (1971) determined that the  $K_{vsi}$  method for carbon dioxide gave unsatisfactory results. The API Data Book shows the  $K_{vsi}$  values for nitrogen to be only a function of pressure, without regard for temperature; Daubert (Personal

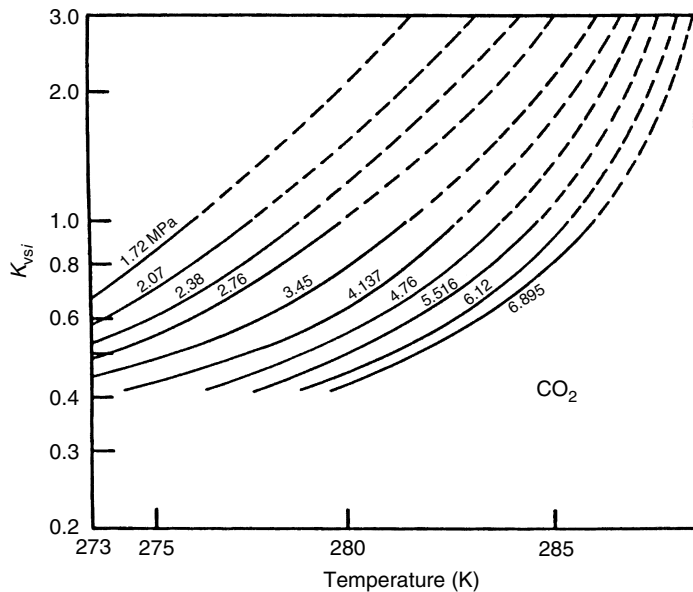


**FIGURE 4.15** Carbon dioxide  $K_{vsi}$  chart. (Reproduced from Unruh, C.H., Katz, D.L., *Trans. AIME*, **186**, 83 (1949). With permission from the American Institute of Mining, Metallurgical, and Petroleum Engineers.)

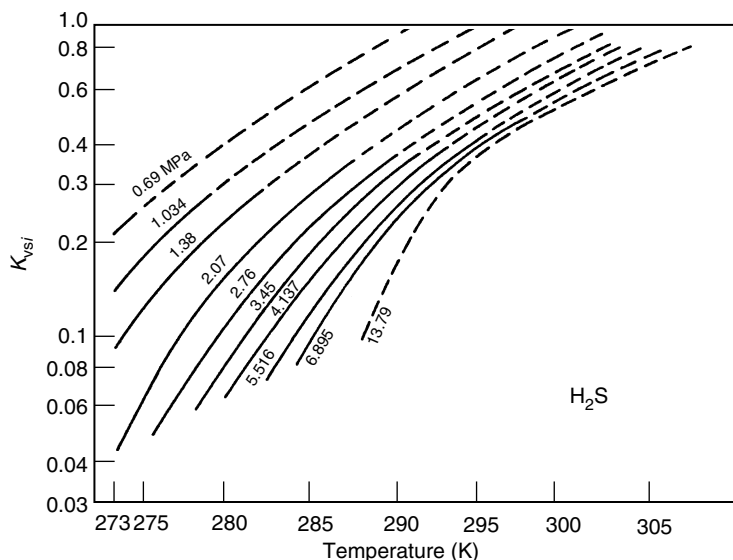


**FIGURE 4.16** Hydrogen sulfide  $K_{vsi}$  chart. (Reproduced from Noaker, L.J., Katz, D.L., *Trans. AIME*, **201**, 237 (1954). With permission from the American Institute of Mining, Metallurgical, and Petroleum Engineers.)

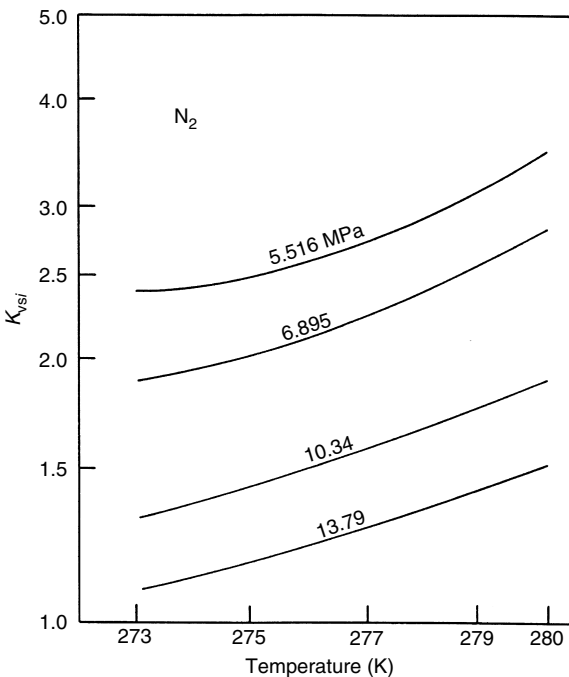


**FIGURE 4.17** Nitrogen  $K_{vsi}$  chart. (Reproduced from Jhaveri, J., Robinson, D.B., *Can. J. Chem. Eng.*, **43**, 75 (1965). With permission from the Canadian Society for Chemical Engineering.)

Communication, June 8, 1987) indicated that data were insufficient for temperature dependence over a wide range of conditions.

It should be thermodynamically impossible for one set of  $K_{vsi}$  charts to serve both hydrate structures (sI and sII), due to different energies of formation. That is, the  $K_{vsi}$  at a given temperature for methane in a mixture of sI formers cannot be the same as that for methane in a mixture of sII formers because the crystal structures differ dramatically. Different crystal structures result in different  $x_{si}$  values that are the denominator of  $K_{vsi}$  ( $\equiv y_i/x_{si}$ ). However, the Katz  $K_{vsi}$  charts do not allow for this possibility because they were generated before the two crystal structures were known. The inaccuracy may be lessened because, in addition to the major component methane, most natural gases contain small amounts of components such as ethane, propane, and isobutane, which cause sII to predominate in production/transportation/processing applications.

More properly a set of charts should be specified for each crystal structure, as was done by Mann et al. (1989). That work included a separate set of  $K_{vsi}$  charts for each of two (sI and sII) hydrate structures, but without a substantial increase in accuracy beyond the original charts.

Another estimation of accuracy may be obtained from Figures 4.18 and 4.19 that compare Katz's  $K_{vsi}$  values with  $K_{vsi}$  values obtained from the methods of

**TABLE 4.4a**  
**Parameters of Equation 4.2**

Component	A	B	C	D	E
CH <sub>4</sub>	1.63636	0.0	0.0	31.6621	-49.3534
C <sub>2</sub> H <sub>6</sub>	6.41934	0.0	0.0	-290.283	2629.10
C <sub>3</sub> H <sub>8</sub>	-7.8499	0.0	0.0	47.056	0.0
i-C <sub>4</sub> H <sub>10</sub>	-2.17137	0.0	0.0	0.0	0.0
n-C <sub>4</sub> H <sub>10</sub>	-37.211	0.86564	0.0	732.20	0.0
N <sub>2</sub>	1.78857	0.0	-0.001356	-6.187	0.0
CO <sub>2</sub>	9.0242	0.0	0.0	-207.033	0.0
H <sub>2</sub> S	-4.7071	0.06192	0.0	82.627	0.0
Component	F	G	H	I	
CH <sub>4</sub>	-5.31E-6	0.0	0.0	0.128525	
C <sub>2</sub> H <sub>6</sub>	0.0	0.0	-9.0E-8	0.129759	
C <sub>3</sub> H <sub>8</sub>	-1.17E-6	7.145E-4	0.0	0.0	
i-C <sub>4</sub> H <sub>10</sub>	0.0	1.251E-3	1.0E-8	0.166097	
n-C <sub>4</sub> H <sub>10</sub>	0.0	0.0	9.37E-6	-1.07657	
N <sub>2</sub>	0.0	0.0	2.5E-7	0.0	
CO <sub>2</sub>	4.66E-5	-6.992E-3	-2.89E-6	-6.223E-3	
H <sub>2</sub> S	-7.39E-6	0.0	0.0	0.240869	
Component	J	K	L	M	N
CH <sub>4</sub>	-0.78338	0.0	0.0	0.0	-5.3569
C <sub>2</sub> H <sub>6</sub>	-1.19703	-8.46E4	-71.0352	0.596404	-4.7437
C <sub>3</sub> H <sub>8</sub>	0.12348	1.669E4	0.0	0.23319	0.0
i-C <sub>4</sub> H <sub>10</sub>	-2.75945	0.0	0.0	0.0	0.0
n-C <sub>4</sub> H <sub>10</sub>	0.0	0.0	-66.221	0.0	0.0
N <sub>2</sub>	0.0	0.0	0.0	0.0	0.0
CO <sub>2</sub>	0.0	0.0	0.0	0.27098	0.0
H <sub>2</sub> S	-0.64405	0.0	0.0	0.0	-12.704
Component	O	Q	R	S	Correlation coefficient
CH <sub>4</sub>	0.0	-2.3E-7	-2.0E-8	0.0	0.999
C <sub>2</sub> H <sub>6</sub>	7.82E4	0.0	0.0	0.0	0.998
C <sub>3</sub> H <sub>8</sub>	-4.48E4	5.5E-6	0.0	0.0	0.998
i-C <sub>4</sub> H <sub>10</sub>	-8.84E2	0.0	-5.4E-7	-1.0E-8	0.999
n-C <sub>4</sub> H <sub>10</sub>	9.17E5	0.0	4.98E-6	-1.26E-6	0.996
N <sub>2</sub>	5.87E5	0.0	1.0E-8	1.1E-7	0.999
CO <sub>2</sub>	0.0	8.82E-5	2.55E-6	0.0	0.996
H <sub>2</sub> S	0.0	-1.3E-6	0.0	0.0	0.999

*Note:* The n-C<sub>4</sub>H<sub>10</sub> conditions should only be evaluated for formation with at least one, smaller guest component.

**TABLE 4.4b**  
**Accuracy of Predictions Using Equation 4.2**

Prediction of hydrate	Temperature (K)	Pressure (kPa)
Number of data predicted	559	583
Percentage convergence, %	71.1	51.3
Absolute average deviation, %	8.13	17.2

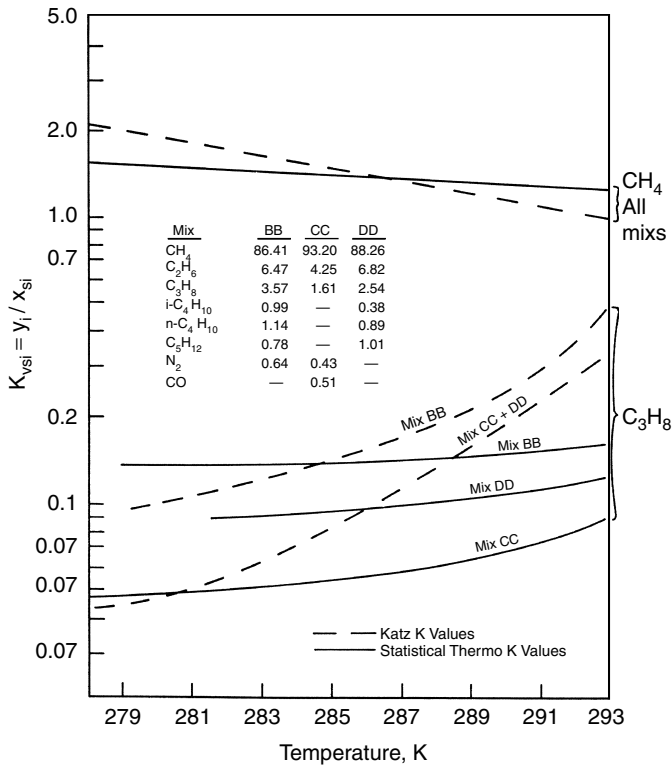


**FIGURE 4.18**  $K_{vsi}$  values for methane and propane from Chapter 4 Katz charts (dashed lines) and Chapter 5 statistical method (solid lines). (Reproduced from Sloan, E.D., in *Proc. 63rd Annual Convention of Gas Processors Association*, **63**, 163 (1984). With permission from the Gas Processors Association.)

Chapter 5, for three natural gases studied by Deaton and Frost (1946). In the figures, the  $K_{vsi}$  values are presented as functions of temperature, with gas compositions as parameters. While both methods predict the three-phase pressure and temperature conditions acceptably, it is important to note that there are substantial differences in the  $K_{vsi}$  values by each method.

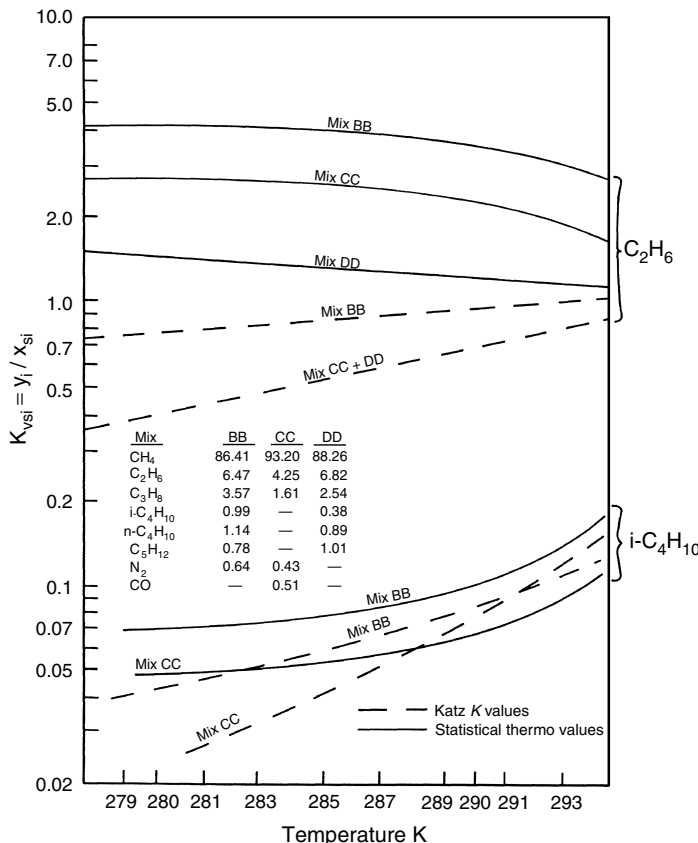


**FIGURE 4.19**  $K_{vsi}$  values for ethane and isobutane from Chapter 4 Katz charts (dashed lines) and Chapter 5 statistical method (solid lines). (Reproduced from Sloan, E.D., in *Proc. 63rd Annual Convention of Gas Processors Association*, **63**, 163 (1984). With permission from the Gas Processors Association.)

In particular, the methane  $K_{vsi}$  values of Carson and Katz are more accurate than those of the other components, suggesting that the charts' longevity is because methane is the major component of a natural gas. The differences in the  $K_{vsi}$  values shown in Figures 4.18 and 4.19 suggest that the charts be used with caution, particularly for gases with significant amounts of either heavy or noncombustible components.

A second limitation to the  $K_{vsi}$ -value charts occurs in the limited range of temperatures above the ice point. Table 4.5 presents the results of a comparison of the experimental three-phase data for hydrates with the predictions of the  $K_{vsi}$  charts and the predictions from the statistical thermodynamics method in Chapter 5. In addition to the inaccuracies, it should be noted that 28% of the three-phase data could not be predicted via the  $K_{vsi}$  charts, principally due to chart temperature range limitations.

**TABLE 4.5**  
**Accuracy and Applicability of  $K_{vsi}$  Values**  
**Compared Against the Statistical Thermodynamic**  
**Method of Chapter 5**

Total number of data points for 20 natural gases	141
Data points not predictable using the $K_{vsi}$ charts	40 (28%)
Average error <sup>a</sup> comparing predictions to data	
Using the $K_{vsi}$ charts	12.3%
Using the statistical thermodynamics method	5.8%

<sup>a</sup> Average error means average absolute error in pressure for a given temperature.

It should be noted that the use of the  $K_{vsi}$  charts implies that both the gas phase and the hydrate phase can be represented as ideal solutions. This means that the  $K_{vsi}$  of a given component is independent of the other components present, with no interaction between molecules. While the ideal solution model is approximately acceptable for hydrocarbons in the hydrate phase (perhaps because of a shielding effect by the host water cages), the ideal solution assumption is not accurate for a dense gas phase. Mann et al. (1989) indicated that gas gravity may be a viable way of including gas nonidealities as a composition variable.

Even with such limitations, the  $K_{vsi}$ -value method represented a significant advance in hydrate prediction ability. It was conceived prior to the determination of the hydrate crystal structures and it is a fine representation of the intuitive insight that characterizes much of Katz's work. The  $K_{vsi}$ -value method was the first predictive method, and it was used as the basis for the calculations in the gravity method, so it is logical that the  $K_{vsi}$ -value method should be more accurate.

### 4.3 QUADRUPLE POINTS AND EQUILIBRIUM OF THREE CONDENSED PHASES ( $L_W-H-L_{HC}$ )

Both the gas gravity method and the  $K_{vsi}$ -value method enable the estimation of three-phase ( $L_W-H-V$ ) equilibrium between quadruple points  $Q_1$  and  $Q_2$  for mixtures as well as for simple natural gas hydrate formers such as those in Table 4.2.

#### 4.3.1 The Location of the Quadruple Points

The lower quadruple point  $Q_1$  ( $I-L_W-H-V$ ) is located at the intersection of the three-phase  $L_W-H-V$  and the  $I-H-V$  pressure-temperature loci, usually within a degree of the ice point (273.15 K). The intersection temperature closely approximates the ice point because (with the exception of carbon dioxide and hydrogen sulfide) the solubility of hydrate formers in water is normally too small to change the freezing point of water significantly.

The approximate location of the upper quadruple point  $Q_2$  ( $L_w-H-V-L_{HC}$ ) is located by the intersection of the  $L_w-H-V$  line with the  $L_w-V-L_{HC}$  line. The termination of the three-phase ( $L_w-V-L_{HC}$ ) line is the critical point that approximates the two-phase ( $V_{HC}-L_{HC}$ ) critical point of the pure hydrocarbon vapor pressure. As a consequence, the intersection of the pure hydrocarbon vapor pressure with the  $L_w-H-V$  line (determined as in Section 4.2) provides the pressure and temperature of the upper quadruple point  $Q_2$ .

The three-phase ( $L_w-V-L_{HC}$ ) pressure–temperature line is approximated by the vapor pressure ( $V_{HC}-L_{HC}$ ) locus for the pure component due to two effects, both of which are caused by the hydrogen-bond phenomenon described in [Chapter 2](#). First, hydrogen bonds cause almost complete immiscibility between the hydrocarbon liquid and the aqueous liquid, so that the total pressure may be closely approximated by the sum of the vapor pressures of the hydrocarbon phase and that of water. Second, hydrogen bonds cause such a self-attraction of the water molecules that the water vapor pressure is very low, composing only a small fraction of the total vapor pressure at any temperature. Because each immiscible liquid phase essentially exerts its own vapor pressure, and because the water vapor pressure is very small, the hydrocarbon vapor pressure is a very good approximation of the three-phase ( $L_w-V-L_{HC}$ ) locus.

### 4.3.2 Condensed Three-Phase Equilibrium

Katz (1972) first noted that hydrates could form from heavy liquids such as crude oils that have dissolved gases suitable for hydrate formation. He suggested that the point of hydrate formation from water and a liquid hydrocarbon phase (no gas present) could be predicted using the vapor–hydrate distribution coefficient  $K_{vsi}$  of Equation 4.1 together with the more common vapor–liquid distribution coefficient  $K_{vli}$  ( $\equiv y_i/x_{li}$ ). In this case Equation 4.3 becomes:

$$\sum_{i=1}^n \frac{y_i}{K_{vsi}} = \sum_{i=1}^n \frac{x_{li} K_{vli}}{K_{vsi}} = 1.0 \quad (4.3a)$$

The substitution of  $y_i = x_{li} \cdot K_{vli}$  in the numerator of Equation 4.3a suggests that this equation applies at the bubble point, or the quadruple point ( $L_w-H-V-L_{HC}$ ) that marks the lowest pressure of a three-phase ( $L_w-H-L_{HC}$ ) region (point C in [Figure 4.2c](#)). The  $P-T$  locus of the three-phase ( $L_w-H-L_{HC}$ ) line is almost vertical, so Equation 4.3a is an approximation of both the lowest pressure and the highest temperature for the three phases in equilibrium. Katz noted that Scauzillo (1956) had measured systems that did not appear to conform to the above equation. Later measurements by Verma (1974) and Holder (1976) confirmed Katz's analysis for hydrate formation from crude oil reservoirs.

For condensed three-phase ( $L_w-H-L_{HC}$ ) hydrate equilibrium, at pressures above the upper quadruple point, the pressure changes extremely rapidly with only a small change in temperature. This is because all three phases are relatively

incompressible, so that only a small temperature change is needed to cause a large pressure change. As a consequence, determination of a condensed phase  $P$ - $T$  locus is a stringent test for even the most accurate equation-of-state to predict both density and mutual solubility of the hydrocarbon and the aqueous phases. As a first approximation, the incompressible three-phase ( $L_w$ - $H$ - $L_{HC}$ ) condition can be estimated by a vertical line on the pressure-temperature plot. Figure 4.1 shows the condensed phase  $P$ - $T$  plot above  $Q_2$  to be almost vertical for simple hydrate formers of natural gas hydrocarbons. The fact that the three-phase ( $L_w$ - $H$ - $L_{HC}$ ) equilibrium can be approximated by a line of infinite slope on a  $P$ - $T$  diagram led nineteenth century investigators to suggest that the upper quadruple point  $Q_2$  represented the maximum temperature of hydration formation.

As noted in Section 4.1.1, without an upper quadruple point methane and nitrogen hydrates are considered to have no upper temperature of formation. The pure component critical temperatures of methane and nitrogen (190.6 and 126.2 K, respectively) negate any possible intersection of their vapor pressures with the three-phase  $L_w$ - $H$ - $V$  loci. It should be noted that the above is a good rule of thumb at normally encountered temperature and pressures. At very high pressures (>500 bar) nitrogen has been determined to have unusual phase behavior. Schouten and coworkers (van Hinsberg et al., 1993, 1994) have measured a nitrogen phase transition ( $sII \Rightarrow sI$ ) at high pressures (to 2 GPa). Kuhs et al. (1996) indicate that at pressures above 500 bar nitrogen can doubly occupy the large cage of  $sII$ . Similarly, data compiled by Ballard and Sloan (2004) show that methane hydrates do have a maximum temperature of formation at 321 K.

However, the condensed three-phase  $P$ - $T$  locus is not exactly vertical. Ng and Robinson (1977) measured the  $L_w$ - $H$ - $L_{HC}$  equilibrium for a number of structure II hydrate mixtures and suggested that a better estimation of the slope  $dP/dT$  might be obtained through the Clapeyron equation:

$$\frac{dP}{dT} = \frac{\Delta H}{T \Delta V} \quad (4.4)$$

where  $\Delta H$  and  $\Delta V$  represent the enthalpy and volume, respectively, accompanying the process of conversion of liquid water and liquid hydrocarbon into hydrate. The value of  $\Delta H$  was found to be almost constant at  $65.4 \pm 2.1$  kJ/mol for many gas mixtures. Therefore, to a good approximation, the temperature and volume change [ $\Delta V \equiv V_H - (V_{LW} + V_{LHC})$ ] at the quadruple point  $Q_2$  determines the slope of the condensed phase equilibrium. Of 21 gas mixtures studied by Ng and Robinson in the  $L_w$ - $H$ - $L_{HC}$  region, the value for  $dP/dT$  ranged between 3.4 and 66.3 MPa/K, with an average value of 10.16 MPa/K (840 psig/ $^{\circ}$ F); therefore the large value of  $\Delta H$  causes the slope ( $dP/dT$ ) to be very high in all cases.

For the upper temperature for hydrate formation, Makogon (1981) suggested a better criterion than the location of  $Q_2$  is the  $P$ - $T$  condition at which the density of the combined hydrocarbon and water is equal to that of the hydrate. He assumed

complete liquid immiscibility and used the inverted Clapeyron relation:

$$\frac{dT}{dP} = \frac{T \Delta V}{\Delta H_H} \quad (4.5)$$

where

$\Delta H_H$  = heat of hydrate formation from liquid water and liquid hydrocarbon<sup>2</sup>

$\Delta V$  = the molar volume of the hydrate less than that of the hydrocarbon and liquid water ( $\equiv V_H - V_{LHC} - V_{LW}$ ).

Since the value of  $\Delta H_H$  remains constant over a large range of pressures, the maximum in  $T$  is determined by the point at which the molar volume change is zero. The volume comparison must be made between the pure liquid hydrocarbon, liquid water, and hydrate, since the hydrocarbon must exist as liquid at pressures between the vapor pressure and the critical pressure. Maxima in hydrate formation temperatures above  $Q_2$  have been calculated, but they have yet to be measured.

#### 4.4 EFFECT OF THERMODYNAMIC INHIBITORS ON HYDRATE FORMATION

Several means of hydrate prevention and dissociation are discussed in detail in [Chapter 8](#). In the present section we consider the lowering of the three-phase (L<sub>w</sub>-H-V) temperature or the increase of the L<sub>w</sub>-H-V pressure via an inhibitor. In this section we consider only thermodynamic inhibitors such as alcohols, glycols, or salts. For kinetic inhibition using LDHIs, such as KIs or AAs, the reader is referred to Chapter 8.

By Gibbs' Phase Rule illustrated in this chapter's introduction, a second intensive variable is needed (in addition to either temperature or pressure) to specify the three-phase binary system with an inhibitor ( $F = 3 - 3 + 2$ ). Typically, the concentration of the inhibitor in the free water phase is specified as the second intensive variable. Substances that have considerable solubility in the aqueous phase, such as alcohols, glycols, and salts, normally act as inhibitors to hydrate formation. The colligative mechanism of formation inhibition is aided by increased competition for water molecules by the dissolved inhibitor molecule or ion through hydrogen bonding for alcohols or glycols, or via Coulombic forces (for salt ions).

As a first approximation, the temperature depression for hydrate inhibition might be considered to be similar to the depression of the freezing point of ice by an equivalent mass fraction of the inhibitor. However, Nielsen and Bucklin (1983) derived an equation indicating that the hydrate depression temperature will always be less than the ice depression temperature by a factor equal to [(heat of fusion of ice)/(heat of hydrate dissociation)], which has a numerical value between 0.6 and 0.7 as a function of the hydrate structure. This is illustrated in [Figure 4.2d](#), by the fact that at constant pressure, the ice depression temperature (i.e., distance between

---

<sup>2</sup>The translation of Makogon's work indicates hydrocarbon vapor, but the condensed hydrocarbon phase is clearly required by the pressure and temperature conditions.

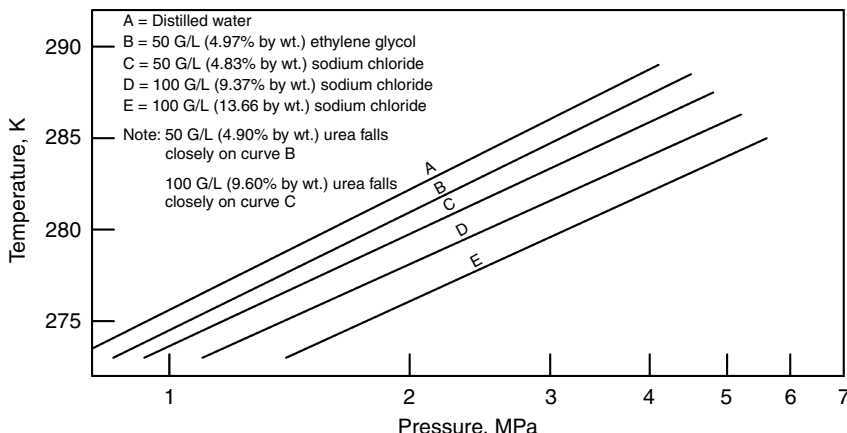


**FIGURE 4.20** Hydrate equilibrium curves with various inhibitors. (Reproduced courtesy of the United States Bureau of Mines (Deaton and Frost, 1946).)

the lower, almost vertical lines) is always greater than the constant pressure distance between the slanted lines, for an equivalent amount of methanol.

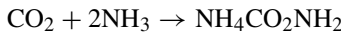
Figure 4.20 shows the correlation of experimental data of Hammerschmidt (1939) with five inhibitors with the pressure and temperature axes reversed from their normal position. The striking feature of Figure 4.20 is the parallel nature of all experimental lines, for the inhibition effect of both alcohols and salts relative to pure water. The parallel solid lines provide some indication of the molecular nature of the inhibition. Normally a phase transformation is considered relative to the change in Gibbs free energy defined as:

$$\Delta G \equiv \Delta H - T \Delta S \quad (4.6)$$

The two components of  $\Delta G$  are (1) an energetic part  $\Delta H$  and (2) a structural part  $\Delta S$ , for the equilibrium ( $V + L_w \leftrightarrow H$ ) at constant temperature and pressure. Upon addition of an inhibitor the Gibbs free energy is increased in order for a lower temperature (or higher pressure) to be required for hydrate formation. Using the Clapeyron equation with the data of Figure 4.20 to relate the slope ( $d \ln P / dT$ ) to the enthalpy of formation  $\Delta H$ , one can determine that the value of  $\Delta H$  is relatively constant. Therefore it appears that the energetic effects are not appreciably affected by the inhibitors. In order to increase the Gibbs free energy, the primary effect of the inhibitor is on the structure of the water phase. The inhibitor encourages nonrandomness (structures other than hydrate-like clusters) in the water, in order to be effective.

Several types of inhibitors have been tried, but the glycols and alcohols have proved to be the most successful. As an example, ammonia was initially determined to be twice as effective an inhibitor as methanol; however, over long periods, ammonia reacts with carbon dioxide and water to form ammonium carbonate and

ammonium carbamate through the reactions:



The solid ammonium carbonate and carbamate are much more difficult to remove than the hydrates (Townsend and Reid, 1978, p. 100). The natural gas industry has opted for methanol and glycols, which may be injected into pipelines and processes without undesirable side reactions.

#### 4.4.1 Hydrate Inhibition via Alcohols and Glycols

The alcohols (in the homologous series beginning with methanol and ending with butanol) all hydrogen bond to water with their hydroxyl group. However, as summarized in [Chapter 2](#), a substantial body of work [reviewed by Franks (1973) and Ben Naim (1980)] indicates that the hydrocarbon end of the alcohol molecule causes a clustering effect on water molecules similar to that of hydrate formers. Alcohols therefore have two effects on water that compete with dissolved apolar molecules for clusters: the hydroxyl group hydrogen bonds the water molecules (the major effect), and the hydrocarbon end of the alcohol tends to organize the water into solvent clusters (the lesser effect), in direct competition with the hydrate for guest and host molecules.

Makogon (1981, p. 134) and Berecz and Balla-Achs (1983, p. 102) indicated that methanol can increase the temperature of hydrate formation at concentrations less than 5 mass% (presumably due to the clustering effect), but higher concentrations inhibit formation. Nakayama and Hashimoto (1980) also suggested that several of the alcohols could form hydrates; yet further study by Nakayama et al. (1997) caused the opposite opinion. Further measurements by Svartas (1988) also indicated that small methanol amounts do not increase hydrate thermodynamic stability.

Wallqvist (1991, 1992) simulated methanol in hydrate cages at very short times (1 ns) and showed that a 4 wt% methanol solution was stable but a 7% solution melted. Koga (1995), Koga et al. (1994a,b), and Koga and Tanaka (1996) simulated hydrate hydrogen bonding of methylamine and methanol guests at times of 100 ps. The increase in the partial charge on the hydrogen atom causes methanol hydrates to be unstable, but methyl amine hydrates are stabilized.

Of alcohols, methanol has been the most popular inhibitor, due to its cost and its effectiveness. Katz et al. (1959, p. 218) indicated that the inhibition ability of alcohols increases with volatility, that is, methanol > ethanol > isopropanol. Typically methanol is vaporized into the gas stream of a transmission line, then dissolves in any free water accumulation(s) where hydrate formation is prevented. Makogon (1981, p. 133) noted that in 1972 the Soviet gas industry used 0.3 kg of methanol for every 1000 m<sup>3</sup> of gas extracted. Stange et al. (1989) indicated that North Sea methanol usage may surpass the ratio given by Makogon by an order

of magnitude. Nielsen and Bucklin (1983) present calculations to indicate that methanol injection in a gas processing turboexpander plant is less expensive than drying with either alumina or molecular sieves. Nevertheless, the use of methanol has become so expensive that methanol recovery and return lines are becoming more common. Some refiners have placed a surcharge of >\$5/bbl on any liquids that have methanol contamination.

The glycols [EG or MEG, diethylene glycol (DEG), and triethylene glycol (TEG)] provide more hydrogen bonding opportunity with water through one more hydroxyl group than alcohols, as well as through oxygen atoms in the case of the larger glycols. The glycols generally have higher molecular weights with lower volatility, so they may be recovered and recycled more from processing/transmission equipment. For gas dominated systems, MEG is frequently preferred to methanol due to recovery.

In a comprehensive set of experimental studies, Ng and Robinson (1983) determined that methanol inhibited hydrate formation more than an equivalent mass fraction of glycol in the aqueous liquid. The preference for methanol versus glycol may also be determined by economic considerations (Nelson, 1973). However, in many North Sea applications ethylene glycol is the preferred inhibition method.

Techniques for hydrate inhibition deal with the methanol concentration in the aqueous liquid in equilibrium with hydrate at a given temperature and pressure. The user also must determine the amount of methanol to be injected in the vapor. This problem was addressed first by Jacoby (1953) and then by Nielsen and Bucklin (1983), who presented a revised methanol injection calculation. The most recent data are by Ng and Chen (1995) for distribution of methanol in three phases: (1) the vapor phase, (2) the aqueous phase, and (3) the liquid hydrocarbon phase.

To approximate the hydrate depression temperature for several inhibitors in the aqueous liquid, the natural gas industry uses the original Hammerschmidt (1939) expression to this day as a check:

$$\Delta T = \frac{2335W}{100M - MW} \quad (4.7)$$

where

$\Delta T$  = hydrate depression, °F

$M$  = molecular weight of the alcohol or glycol

$W$  = wt% of the inhibitor in the liquid.

Equation 4.7 was based on more than 100 experimental determinations of equilibrium temperature lowering in a given natural gas–water system in the inhibition concentration range of 5–25 wt% of the free water. The equation was used to correlate data for alcohols and ammonia inhibitors. Hammerschmidt (1939) provided for a modification of the molecular weight  $M$  when salts were used as inhibitors. Unfortunately, no information on the gas composition and no listing of the individual experimental data were provided. The assumption is normally made that the gases used by Hammerschmidt were methane-rich.

**TABLE 4.6**  
**Comparison of Two Simple Prediction Methods for Hydrate Inhibition by Methanol**

Simple component	Wt% MeOH	Number of hydrate data points	Average % error in temperature by	
			Hammerschmidt Equation 4.7	Freezing point depression
Methane	10	4	3.98	4.21
Methane	20	3	7.56	15.3
Ethane	10	5	2.03	8.97
Ethane	20	2	1.26	23.5
Propane	5	3	1.62	3.13
Carbon dioxide	10	3	7.63	3.53

Pieroen (1955) and Nielsen and Bucklin (1983) presented derivations to show the theoretical validity of the Hammerschmidt equation. The latter work suggested that the equation applies only to typical natural gases, and to methanol concentrations less than 0.20 mole fraction (typically for system operation at temperatures above 250 K). It may easily be shown (Yamanlar et al., 1991) that the Hammerschmidt equation should not apply to high concentrations of an inhibitor that might vaporize. Nixdorf and Oelrich (1996) have shown that the Hammerschmidt equation under-predicts natural gas systems inhibited with TEG.

Due to a cancellation of errors, the equation (without modification) is applicable for aqueous ethylene glycol concentrations to about 0.40 mole fraction (typically for system operation to 233 K). A comparison of results from Hammerschmidt's equation, as well as the prediction by the freezing point depression of water for methanol inhibition is summarized in Table 4.6.

Nielsen and Bucklin (1983) presented an improved version of the Hammerschmidt equation which is accurate over a wider range, that is, to concentrations as large as 0.8 mole fraction. They suggested that Equation 4.8 may be effectively used to design methanol injection systems operating as low as 165 K.

$$\Delta T = -129.6 \ell \ln(1 - x_{\text{MeOH}}) \quad (4.8)$$

where  $\Delta T$  is the hydrate temperature depression below the uninhibited condition, in °F. Makogon (1981, p. 134) indicated that the inhibition effect is a function (albeit much smaller) of pressure as well as that of temperature.

An important recent development is the consideration of under-inhibited systems, as reported by Austvik and coworkers, (Austvik et al., 1995; Gjertsen et al., 1996). Yousif et al. (1996) measured two adverse effects of small amounts of methanol on hydrate inhibition: (1) insufficient inhibition with methanol enhances the rate and amount of hydrates that form and (2) hydrates that form with

small amounts of methanol adhere to surfaces more than those formed in the absence of methanol. At under-inhibited amounts of methanol, MEG, and salt, hydrates coated the pipe wall more, both in field and in laboratory studies. This suggests that pipeline plugging may be worse in under-inhibited systems than if no thermodynamic inhibitor were added.

#### 4.4.2 Hydrate Inhibition Using Salts

The action of salts as inhibitors is somewhat different than that of alcohols or glycols. The salt ionizes in solution and interacts with the dipoles of the water molecules with a much stronger Coulombic bond than either the hydrogen bond or the van der Waals forces that cause clustering around the apolar solute molecule. The stronger bonds of water with salt ions inhibit hydrate formation; water is attracted to ions more than water is attracted to the hydrate structure.

As a secondary effect, this clustering also causes a decrease in the solubility of potential hydrate guest molecules in water, a phenomenon known as “salting-out.” Both ion clustering and salting out combine to require substantially more subcooling to overcome the structural changes and cause hydrates to form.

For an accurate estimate of salt effects, the computer program (enclosed with this monograph) should be used, incorporating the methods in [Chapter 5](#), and in the User’s Manual in the book’s CD. However, a rapid estimate for the depression of salt on hydrate equilibrium may be obtained by knowledge of the depression of salt on ice equilibrium, using the method in this section.

Pieroen (1955) provided a theoretical foundation for the Hammerschmidt equation, showing that when the solubility of one phase in the other is neglected, a nonvaporizing inhibitor such as salt can be approximated as

$$\ln a_w = \frac{\Delta H}{nR} \left[ \frac{1}{T_w} - \frac{1}{T_s} \right] \quad (4.9)$$

where  $a_w$  is water activity,  $\Delta H$  is the heat of dissociation of hydrate,  $n$  is the hydration number, and  $T_w$  and  $T_s$  are the hydrate formation temperatures in pure water and the salt solution. Menten et al. (1981) showed that the above equation can be incorporated directly into a hydrate calculation method. More recently, Dickens and Quinby-Hunt (1997) suggested that the above equation could be combined with a similar equation for the formation of ice:

$$\ln a_w = \frac{\Delta H^{\text{fus}}}{R} \left[ \frac{1}{T_f} - \frac{1}{T_{fs}} \right] \quad (4.10)$$

where  $\Delta H^{\text{fus}}$  is the heat of fusion of ice (6008 J/mol),  $T_f$  and  $T_{fs}$  are the freezing point temperatures of water (273.15 K) and water with a salt solution. Equating Equations 4.9 and 4.10 one obtains a simple relation to calculate  $T_s$ , the hydrate

formation temperature in the presence of salt

$$\left[ \frac{1}{T_w} - \frac{1}{T_s} \right] = \frac{6008n}{\Delta H} \left[ \frac{1}{273.15} - \frac{1}{T_{fs}} \right] \quad (4.11)$$

A procedure use of Equation 4.11 is shown in the example below.

### Example 4.5: Short Cut Calculation of Hydrate Formation Conditions with Salt

Calculate the methane hydrate formation temperature at 2.69 MPa with 0.03936 mole fraction sodium chloride in the water phase.

*Solution*

1. At the specified salt concentration (0.03936 mole fraction), determine the freezing point of water ( $T_{fs}$ ) from a handbook, such as the *Handbook of Chemistry and Physics*, as  $T_{fs} = 268.9$  K.
2. Determine the enthalpy of hydrate dissociation to gas and pure water ( $\Delta H$ ) and the hydration number ( $n$ ) at the ice point using the methods of Section 4.6. For methane,  $\Delta H = 54,190$  J/(mol methane) and  $n = 6.0$ .
3. Calculate the coefficient ( $6008n/\Delta H$ ) in Equation 4.11. For methane the value of the coefficient is 0.665.
4. Calculate the three-phase hydrate dissociation temperature,  $T_w$  (without salt), at the pressure of interest using either tabulated data, the equations in Table 4.1, or the  $K_{vsi}$  method. For example, the methane three-phase temperature at 2.69 MPa is 273.3 K, as measured by de Roo et al. (1983).
5. Calculate the hydrate dissociation temperature  $T_s$  in the presence of salt using Equation 4.11. Equation 4.11 predicts the dissociation temperature to be 270.45 K. De Roo et al. (1983) measured the dissociation temperature as 268.3 K.

While Equation 4.11 provides a simple accurate method to estimate the effects of salt, the following points should be noted:

1. Equation 4.11 does not contain pressure explicitly. If Equation 4.11 is recast as:

$$\frac{\Delta T^{\text{hyd}}}{T_w T_s} = K \frac{\Delta T^{\text{fus}}}{T_f T_{fs}} \quad (4.12)$$

then the  $\Delta T^{\text{hyd}}$  may be constant over a wide range of pressures, because  $K$  is the constant shown in Equation 4.11.

2. The hydrate temperature depression will always be less than the ice temperature depression  $\Delta T^{\text{fus}}$ , since the value of  $\Delta H/n$  in Equation 4.9 is always greater than  $\Delta H^{\text{fus}}$  in Equation 4.10. In the case of Example 4.5 the  $\Delta T^{\text{hyd}}$  is 66.5% of the value of  $\Delta T^{\text{fus}}$ .
3. The hydration number  $n$  and the heat of dissociation  $\Delta H$  change as a function of the components, as indicated in Section 4.6.
4. The method can be extended to salt mixtures, if the freezing point depression of water is known for the mixture. Patwardhan and Kumar (1986) suggest a simple extension to determine water activities for mixed salts from single salt activities, such as in Equations 4.9 and 4.10.

## 4.5 TWO-PHASE EQUILIBRIUM: HYDRATES WITH ONE OTHER PHASE

Hydrates may also exist in equilibrium with only a fluid hydrocarbon phase (either vapor or liquid) when there is no aqueous phase present. Two-phase (H–V or H–L<sub>HC</sub>) regions are shown in the  $T$ – $x$  diagram of Figure 4.3. Similarly, Figure 4.3 shows the L<sub>w</sub>–H region for hydrates in equilibrium with water containing a small amount of dissolved methane, as in the case for hydrate formation in oceans, as exemplified in Chapter 7.

By the Gibbs' Phase Rule illustrated in the introduction to this chapter, in the three-phase regions, of Sections 4.2 through 4.4, only one intensive variable is needed to specify a binary system; that is, specifying  $T$  determines  $P$ , and vice versa for a fixed gas composition. However, two variables are needed to specify a two-phase binary system; typically water concentration in the hydrocarbon fluid is specified as the second variable at a specified temperature or pressure. The determination of the equilibrium water concentration enables the engineer to maintain the hydrocarbon fluid in the single-phase region, without hydrate solid formation for fouling or flow obstruction. Similarly, for L<sub>w</sub>–H equilibria, the methane solubility in water determines when hydrates will be stable, as shown in Section 7.3.3.

Two common misconceptions exist concerning the presence of water to form hydrates in pipelines, both of which are illustrated via the  $T$ – $x$  phase equilibrium diagrams in Figure 4.3. The first and most common misconception is that a free water phase is absolutely necessary for the formation of hydrates. The upper three-phase (L<sub>w</sub>–H–V) line temperature marks the condition of hydrate formation from free water and gas. Below that temperature and to the right of the hydrate line, however, are two-phase regions in which hydrates are in equilibrium only with hydrocarbon vapor or liquid containing a small (<1000 ppm) amount of water.

From a strict thermodynamic standpoint then, a vapor or liquid (with dissolved water) can form hydrates at the H–V or the H–L<sub>HC</sub> boundaries without a free water phase. The question of the accumulation of a hydrate phase is a question of kinetics,

dependent upon the time necessary for hydrate nuclei to attain a critical size. This time may be in excess of that available for laboratory study, but may occur in processes that operate over extended periods of days, months, or years.

In addition there have been multiple studies (Sloan et al., 1976; Cady, 1983a,b; Kobayashi et al., 1987; Woolridge et al., 1987) that demonstrate that hydrate growth can occur from a hydrocarbon fluid phase if a hydrate nucleus is either already present, absorbed at sites on a wall, or on a third surface.

From an operator's perspective, if a dehydrator abnormality enables free water to enter a vessel or pipeline, then that free water can readily form hydrates, so that additional saturated vapor (without free water) will cause that initial hydrate mass to grow. Therefore, from a practical standpoint one should require that the hydrocarbon fluid be maintained in the thermodynamic single-phase region if hydrates are to be prevented.

The second misconception about two-phase hydrates concerns the dew point of the hydrocarbon phase. Bucklin et al. (1985) correctly indicate that the extrapolated points from the vapor–liquid water region at higher temperatures give metastable dew points. This effect is indicated in the *Gas Processors Association Handbook* (1981, Figure 15.14). However, it is also incorrect to determine the dew point, assuming that ice is the condensed water phase; such equilibrium occurs relatively rarely. Much more frequently, hydrate is the condensed water phase at low temperature or high pressure. Details of vapor–hydrate equilibrium are given in Section 4.5.1, while the liquid hydrocarbon–hydrate equilibrium is described in Section 4.5.2. [Chapter 8](#) discusses production/transmission/processing implications of these equilibria.

#### 4.5.1 Water Content of Vapor in Equilibrium with Hydrate

The water content of the vapor phase in (H–V) equilibrium is very small (typically less than 0.001 mole fraction) and therefore difficult to measure accurately. As a consequence, in the history of gas processing, semilogarithmic straight lines (gas water content versus reciprocal absolute temperature) from the L<sub>w</sub>–V region were extrapolated into the H–V region with limited justification.

A typical chart for water content from this period is presented in [Figure 4.21](#). In Figure 4.21 the water content chart at temperatures above the hydrate stability conditions is based primarily on the data of Olds et al. (1942) while the data of Skinner (1948) were the basis for extrapolations to temperatures below the hydrate formation point. A summary chart is given by McKetta and Wehe (1958). However, below the initial hydrate formation conditions, Figure 4.21 represents metastable values, as observed in gas field data by Records and Seely (1951). Kobayashi and Katz (1955) indicated that such concentration extrapolations across hydrate phase boundaries yield severe errors.

Laboratory confirmation that the water content of gas in equilibrium with hydrate should be much lower than the extrapolated values has been verified by Sloan et al. (1976) for methane hydrates, and by Song and Kobayashi (1982) for

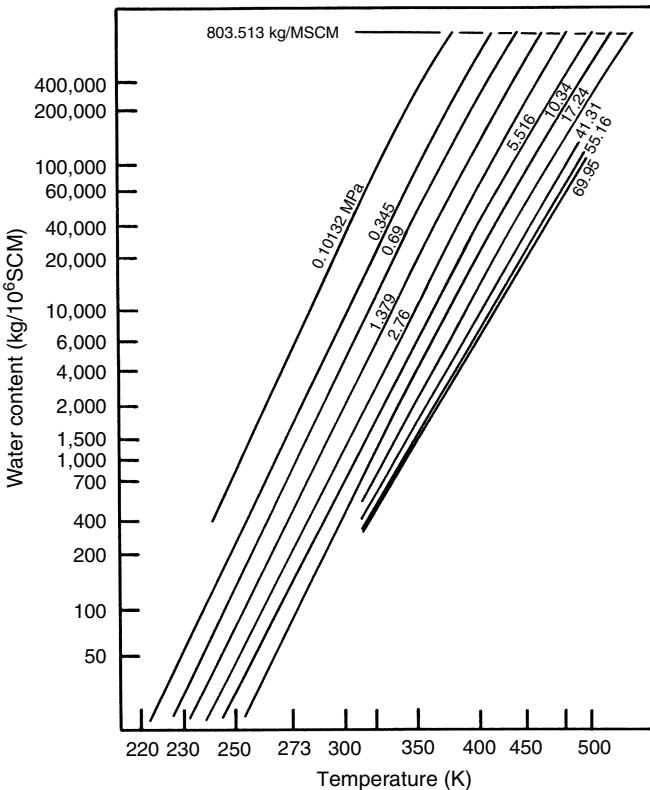


**FIGURE 4.21** Metastable water content of gas. (Reproduced, from Kobayashi, R., Song, K.Y., Sloan, E.D., in *Petroleum Engineering Handbook* (1987). With permission from the Society of Petroleum Engineers.)

methane–propane hydrates. A typical replacement chart is shown in Figure 4.22. In this figure the high temperature L<sub>W</sub>–V region is separated from the low temperature H–V region by a line representing the three-phase (L<sub>W</sub>–H–V) boundary.

The isobaric data in the vapor–hydrate region of Figure 4.22 follow semilogarithmic straight lines when water content is plotted against reciprocal absolute temperature, but these lines have slopes different from the straight lines in the L<sub>W</sub>–V region. In addition, the three-phase (L<sub>W</sub>–H–V) point at which the slope change occurs is a function of gas composition. The change in the slope of an isobar from the L<sub>W</sub>–V region occurs at different temperatures for differing compositions.

With the above complexities, a comprehensive water content chart (or series of charts) for gases of differing compositions would be problematic. Further, the data are so sparse that mathematical methods for determining the water content of gases in the V–H region should be considered to fit to a small amount

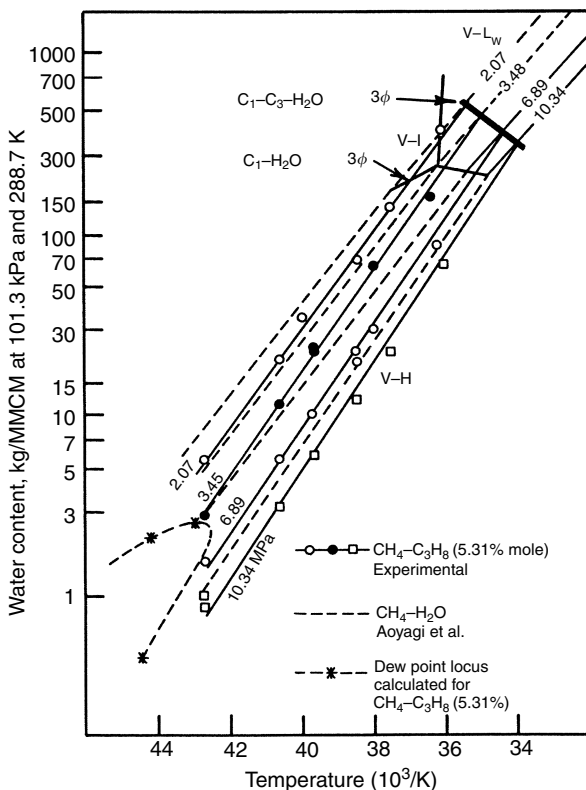


**FIGURE 4.22** Equilibrium water content chart for methane (dashed) and for methane + 5.31% propane (solid). (Reproduced from Song, K.Y., Kobayashi, R., *Ind. Eng. Chem. Fund.*, **21**, 391 (1982). With permission from the American Chemical Society.)

of data, and should be regarded with some suspicion. A more thermodynamically correct calculation method for interpolation of the available database is given in Chapter 5, and is available on the computer program CSMGem with this book's CD.

It is worthwhile to emphasize that all of the available data for V-H studies have been for methane-rich gases. For heavier gases, or for noncombustible gases, there are almost no data in the V-H two-phase region; the sole exception is the water content study of Song and Kobayashi (1987) for carbon dioxide.

#### 4.5.2 Water Content of Liquid Hydrocarbon in Equilibrium with Hydrates

In the H-L<sub>HC</sub> two-phase region there is a severe paucity of both data and a simple calculation scheme. These data find applications in condensate pipelines, which may have hydrates. The only data available are from this laboratory

[Sloan et al. (1986, 1987)] with corrections by Song and Kobayashi (1994). A prediction scheme is discussed in [Chapter 5](#) using the statistical thermodynamics method and included in the program CSMGem.

Because there are so few data for water content of the fluid hydrocarbon in either of the two-phase (H–V or H–L<sub>H</sub>C) regions, their accuracy cannot be determined. These data are very difficult to obtain due to the low concentrations (typically <100 ppm mol). The inaccuracies in normal experimental data in other phase regions are frequently greater than the absolute values of the water content in the H–L<sub>H</sub>C region.

With low concentrations of water a substantial amount of time may be required before the water molecules can agglomerate into a hydrate structure. Experimental time to acquire each data point is normally on the order of days or weeks, rather than hours. Appreciable metastability is observed, and long times are required for the formation of critical hydrate nuclei. Nevertheless, the long time involved should not be taken as an indication that hydrates are not thermodynamically stable in the two-phase region. The phase diagram analyses presented in Section 4.1 indicate the thermodynamic validity of this region.

#### 4.5.3 Methane Content of Water in Equilibrium with Hydrates

Data and predictions for methane dissolved in water, solely in equilibrium with hydrates (L<sub>W</sub>–H without a vapor phase) find application in instances such as formation of hydrates in marine systems ([Chapter 7](#)). To date there are only few reliable hydrate data in equilibrium with water containing methane—the data of Servio and Englezos (2002) and Chou et al. (Personal Communication, December 18, 2006), as listed in [Chapter 6](#).

Because there are so few data for the methane content of water in equilibrium with hydrate (L<sub>W</sub>–H) regions, their accuracy cannot be determined. These data are very difficult to obtain due to the low methane concentrations (typically <100 ppm mol). The inaccuracies in normal experimental data in other phase regions are frequently greater than the absolute values of the water content in the L<sub>W</sub>–H region.

As in the previous sections, it is worthwhile to compare these data against the predictions of CSMGem and User Manual, included on the CD in the endpapers, with examples in [Appendix A](#).

### 4.6 HYDRATE ENTHALPY AND HYDRATION NUMBER FROM PHASE EQUILIBRIUM

The enthalpy of hydrate formation of simple natural gas hydrate formers (from gas and water or ice) is given in [Table 4.7](#) taken from the dissertation of Kamath (1984). Note that each component has two temperature regions, above and below the ice point, with a  $\Delta H$  difference related by the heat of fusion at the ice point.

**TABLE 4.7**

**Hydrate Formation Enthalpy for Three-Phase Conditions of Single Natural Gas Components Using  $\Delta H$  [cal/gmol gas] =  $a + b/T$  [K]**

Component	Type	T range (°C)	$a \times 10^{-3}$	b
Methane	Lw–H–V	0 to 25	13.521	-4.02
Methane	I–H–V	-25 to 0	6.534	-11.97
Ethane	Lw–H–V	0 to 14	13.254	-15.00
Ethane	I–H–V	-25 to 0	8.458	-9.59
Propane	Lw–H–V	0 to 5	-37.752	250.09
Propane	I–H–V	-25 to 0	7.609	-4.90
Carbon dioxide	Lw–H–V	0 to 11	19.199	-14.95
Carbon dioxide	I–H–V	-25 to 0	9.290	-12.93
Nitrogen	Lw–H–V	0 to 25	6.188	18.37
Nitrogen	I–H–V	-25 to 0	4.934	-9.04
Hydrogen sulfide	Lw–H–V	0 to 25	6.782	31.45
Hydrogen sulfide	I–H–V	-25 to 0	8.488	-7.81

*Source:* From Kamath, V.A. *Study of Heat Transfer Characteristics During Dissociation of Gas Hydrates in Porous Media*, Ph.D. Dissertation, University of Pittsburgh, University Microfilms No. 8417404, Ann Arbor, MI, 1984. With permission.

The intention of this section is to relate these enthalpies both to the phase equilibrium values and to show how these values relate to microscopic structure and to hydration numbers at the ice point.

#### 4.6.1 The Clausius–Clapeyron Equation and Hydrate Equilibrium

In the most common thermodynamic case, the Clapeyron equation is used with pure components to obtain the heat of vaporization from pure component two-phase (vapor pressure) data. The Clapeyron equation is one of the primary successes of thermodynamics, because it enables the calculation of  $\Delta H$ , which is difficult to measure, from easily available properties of pressure and temperature.

In hydrate equilibrium, it may seem slightly unusual to apply it to binary systems (water and one guest component) of three-phase (Lw–H–V or I–H–V) equilibrium to obtain the heats of dissociation. As van der Waals and Platteeuw (1959b) point out, however, the application of the Clapeyron equation is thermodynamically correct, as long as the system is univariant, as is the case for simple hydrates.

If the volume of hydrate approximates that of water (or ice) in the hydrate formation reaction ( $L_w + V \leftrightarrow H$ ), then to a good approximation,  $\Delta V \approx V_g$  ( $= zRT/P$ , where  $z$  is compressibility). The substitution of this expression for  $\Delta V$

**TABLE 4.8**  
**Accuracy of the Clausius–Clapeyron Equation for Hydrate Heat of Dissociation to Vapor and Water**

Component	$\Delta H$ calculated (kJ/mol gas)	$\Delta H$ measured (kJ/mol gas)
Methane	56.9	54.2
Ethane	71.1	71.8
Propane	126.0	129.2
Isobutane	130.4	133.2

in the Clapeyron equation (Equation 4.4) leads to a more useable form, namely, the Clausius–Clapeyron equation:

$$\frac{d \ln P}{d(1/T)} = -\frac{\Delta H}{zR} \quad (4.13)$$

Semilogarithmic plots of formation pressure versus reciprocal absolute temperature yield straight lines, over limited temperature ranges, for hydrate formation from either liquid water, or ice. From Equation 4.13 such linear plots either indicate (1) relatively constant values of the three factors: (a) heat of formation,  $\Delta H$ , (b) compressibility factor,  $z$ , (c) stoichiometry ratios of water to guest or (2) cancellation of curvilinear behavior in these three factors.

The most recent confirmation of the validity of the Clausius–Clapeyron equation for hydrates was by Handa (1986a,b), who measured the heat of dissociation (via calorimetry) of the normal paraffins that form simple hydrates. Table 4.8 shows Handa's values for hydrate dissociation enthalpy compared to those calculated with the Clausius–Clapeyron equation by Sloan and Fleyfel (1992). The agreement appears to be very good for simple hydrates.

Roberts et al. (1940), Barrer and Edge (1967), Skovborg and Rasmussen (1994) present similar, detailed derivations to consider the use of the Clapeyron equation for hydrate binary and multicomponent systems. The reader is referred to the work of Barrer and Edge (1967) for the precise meaning of  $dP/dT$  and the details of the derivation. Barrer and Stuart (1957) and Barrer (1959) point out that the problem in the use of the Clapeyron equation evolves from the nonstoichiometric nature of the hydrate phase. Fortunately, that problem is not substantial in the case of hydrate equilibrium, because the nonstoichiometry does not change significantly over small temperature ranges. At the ice point, where the hydrate number is usually calculated, the nonstoichiometry is essentially identical for each three-phase system at an infinitesimal departure on either side of the quadruple point.

#### 4.6.1.1 Enthalpy of dissociation and cavity occupation

In this section, enthalpy evidence for structures I, II, and H is presented to suggest that guest size fixes the heat of dissociation. That is, heat of dissociation for the hydrate structure is determined by the cavity occupied. The initial work for sI and sII was presented by Sloan and Fleyfel (1992), with a critique by Skovborg and Rasmussen (1994) and a reply by Sloan and Fleyfel (1994). Similar results for sH are presented by Mehta and Sloan (1996b).

To a fair engineering approximation  $\Delta H_d$  is not only a function of the hydrogen bonds in the crystal, but also a function of cavity occupation. Because the Clausius–Clapeyron equation determines the heat of hydrate formation by the slopes of plots of  $\ln P$  versus  $1/T$ , one may easily determine relationships between heats of dissociation.

The evidence for such a relationship is as follows:

1. The slope of the hydrate dissociation line ( $\ln P$  versus  $1/T$ ) is directly related to the cavity size(s) occupied by the guests, as shown in Figure 4.23.
2. For mixed guests such as  $\text{CH}_4 + \text{C}_2\text{H}_6$ , Figure 4.24 shows that a superimposed identical slope fits all data over a wide range of mixed sI compositions for a value of  $\Delta H = 74 \text{ kJ/mol}$ . Similarly, Figure 4.25 shows that mixtures of  $\text{CH}_4 + \text{C}_3\text{H}_8$  have an identical superimposed

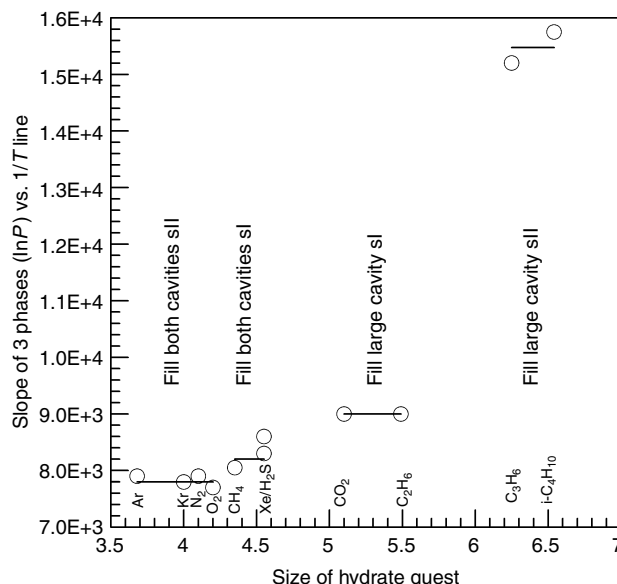


**FIGURE 4.23** Relationship of the slope of the hydrate dissociation line ( $\ln P$  vs.  $1/T$ ) to the cavity size(s) occupied by guests. (Reproduced from Sloan, E.D., Fleyfel, F., *Fluid Phase Equilib.*, **96**, 233 (1994). With permission from Elsevier Science Publishers.)

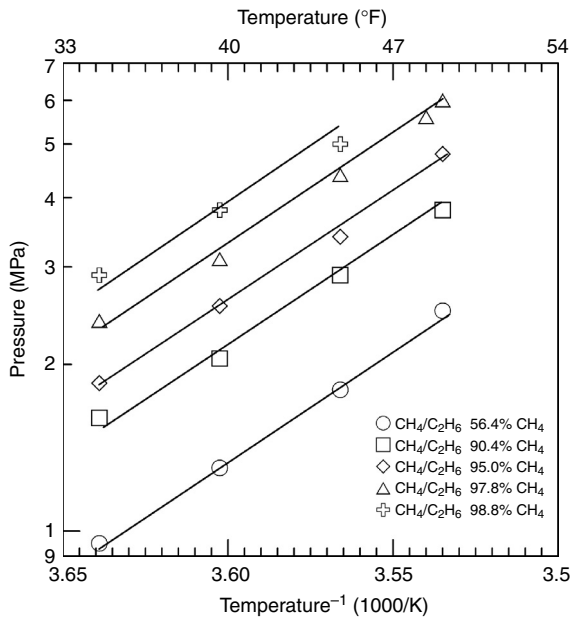


**FIGURE 4.24** Hydrate dissociation lines for mixtures of methane and ethane. (Reproduced from Sloan, E.D., Fleyfel, F., *Fluid Phase Equilib.*, **76**, 123 (1992). With permission from Elsevier Science Publishers.)

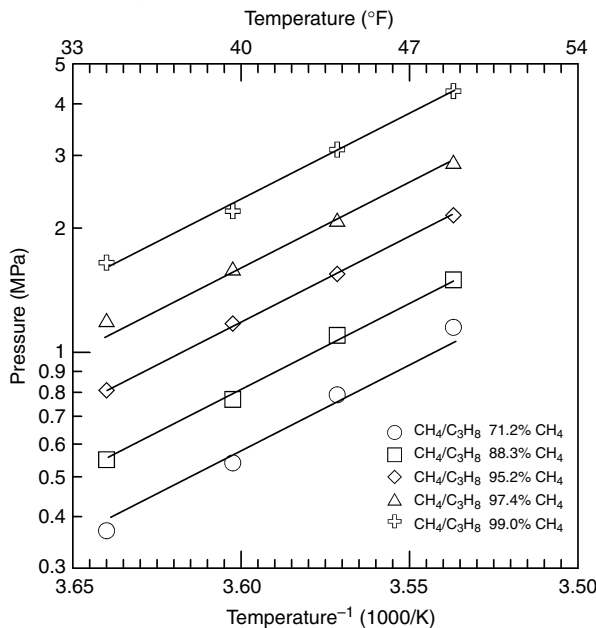


**FIGURE 4.25** Hydrate dissociation lines for mixtures of methane and propane. (Reproduced from Sloan, E.D., Fleyfel, F., *Fluid Phase Equilib.*, **76**, 123 (1992). With permission from Elsevier Science Publishers.)

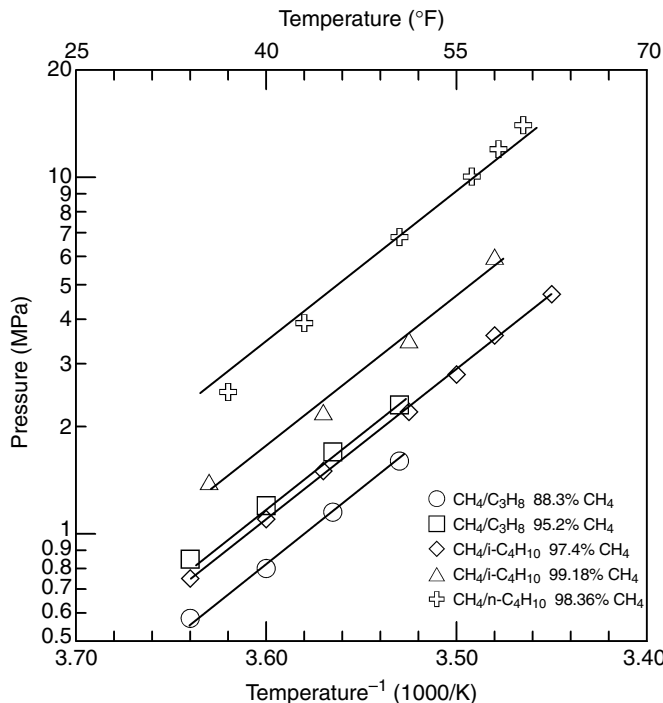


**FIGURE 4.26** Hydrate dissociation lines for mixtures of methane with isobutane and methane with normal butane. (Reproduced from Sloan, E.D., Fleyfel, F., *Fluid Phase Equilibr.*, **76**, 123 (1992). With permission from Elsevier Science Publishers.)

slope over a wide gas composition range for sII hydrate formation yielding a value of  $\Delta H = 79.2 \text{ kJ/mol}$ . As indicated in Chapter 6, mixtures of  $\text{CH}_4 + \text{C}_2\text{H}_6$  form sII hydrates over the concentration range 67–99%  $\text{CH}_4$  even though  $\text{CH}_4$  and  $\text{C}_2\text{H}_6$  simple hydrates each form sI. The difference in the heats (5.2 kJ/mol) for these two mixtures may be within the experimental accuracy.

3. Figure 4.26 shows that semilogarithmic plots for several sII binary mixtures ( $\text{CH}_4 + \text{C}_3\text{H}_8$ ,  $+ n\text{-C}_4\text{H}_{10}$ ,  $+ i\text{-C}_4\text{H}_{10}$ ) can be fit with a superimposed identical slope that is equal to the slope for  $\text{CH}_4 + \text{C}_3\text{H}_8$  shown in Figure 4.25.
4. Figure 4.27 shows that the same slopes for sII hydrate in Figures 4.25 and 4.26 bracket the data for many natural gases.
5. Mehta and Sloan (1996b) present data in Table 4.9 for 19-structure H hydrates formers along univariant four-phase lines. With only three exceptions, the enthalpy of hydrate formation is  $79.5 \text{ kJ/mol} \pm 7\%$ . In each case, methane occupies the  $5^{12}$  and the  $4^3 5^6 6^3$  cages while the larger guest occupies the  $5^{12} 6^8$  cage.

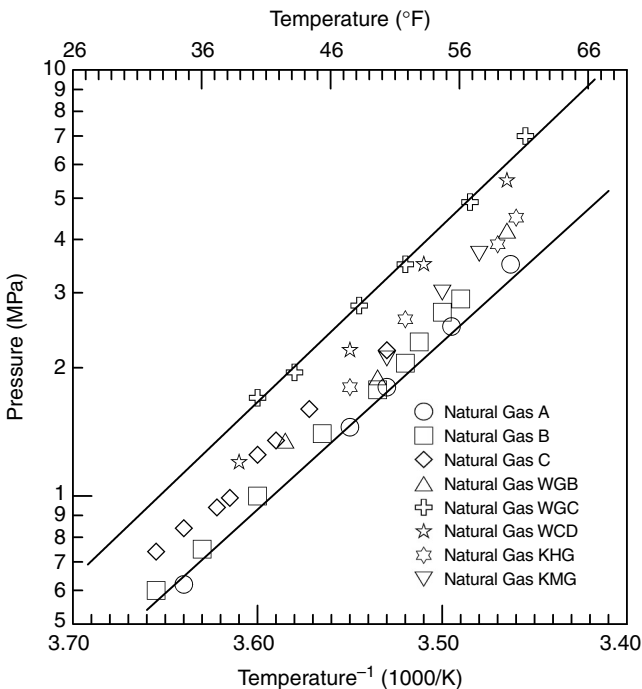


**FIGURE 4.27** Hydrate dissociation lines for natural gases. (Reproduced from Sloan, E.D., Flylefel, F., *Fluid Phase Equilib.*, **76**, 123 (1992). With permission from Elsevier Science Publishers.)

#### 4.6.2 Determination of the Hydration Number

Historically, two periods occurred for the determination of the number of hydrate water molecules per guest molecule. In the first century (1778–1900) after the discovery of hydrates, the hydration number was determined directly. That is, the amounts of hydrated water and guest molecules were each measured via various methods. The encountered experimental difficulties stemmed from two facts: (1) the water phase could not be completely converted to hydrate without some occlusion and (2) the reproducible measurement of the inclusion of guest molecules was hindered by hydrate metastability. As a result, the hydrate numbers differed widely for each substance, with a general reduction in the ratio of water molecules per guest molecule as the methods became refined with time. After an extensive review of experiments of the period, Villard (1895) proposed “Villard’s Rule” to summarize the work of that first century of hydrate research:

The dissociable (hydrate) compounds, that form through the unification of water with different gases and that are only stable in the solid form, all crystallize regularly and have the same constitution that can be expressed by the formula  $M + 6H_2O$ , where  $M$  designates a molecule of the respective gas

**TABLE 4.9**  
**Structure H Heats of Dissociation ( $\Delta H$ ) at 273.15 K**

Guest	-Slope (1/K)	Comp $z_{\text{CH}_4}$	$\Delta H$ (kJ/mol gas)
2-Methylbutane	9,333	0.9310	72.24
2,2-Dimethylbutane	10,118	0.9641	81.10
2,3-Dimethylbutane	10,324	0.9555	82.01
2,2,3-Trimethylbutane	9,289	0.9688	74.66
2,2-Dimethylpentane	8,006	0.9279	61.76
3,3-Dimethylpentane	9,906	0.9584	78.93
Methylcyclopentane	10,384	0.9578	82.68
Ethylcyclopentane	10,632	0.9595	84.81
Methylcyclohexane	10,173	0.9650	81.61
1,1-Dimethylcyclohexane	10,465	0.9750	84.83
cis-1,2-Dimethylcyclohexane	10,161	0.9624	81.30
Cycloheptane	10,568	0.9504	83.50
Cyclooctane	10,568	0.9641	84.70
Adamantane	7,899	0.9579	62.90
Cycloheptene	7,651	0.9508	60.48
cis-Cyclooctene	9,445	0.9616	75.51
2,3-Dimethyl-1-butene	9,709	0.9431	76.12
3,3-Dimethyl-1-butene	9,704	0.9529	76.87
3,3-Dimethyl-1-butyne	9,228	0.9246	70.93

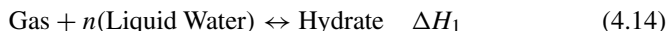
While the above estimate may seem antiquated, Villard's Rule is a good rule of thumb in many cases. Note that if a guest fills all of both cavities in sI and sII, the hydration number would be 5.75 and 5.67, respectively, so a value of 6 allows for the possibility of empty cages, and is frequently taken as a good approximation to the hydration number for methane hydrates. However, Villard's Rule is not a good approximation for components that only fill the large cavity of either sI (e.g., ethane) or sII (e.g., propane).

#### 4.6.2.1 Using the Clapeyron equation to obtain hydration number

After 1900 the direct determination of hydrate number was abandoned in favor of the second, indirect method. The indirect method is still in use today and is based on calculation of the enthalpies of formation of hydrate from gas and water, and from gas and ice. This method was originally proposed by de Forcrand (1902) who used the Clapeyron equation to obtain the heat of dissociation from three-phase, pressure–temperature data, as in the below paragraph. With this more accurate method many exceptions were found to Villard's Rule. The historical summary provided in Chapter 1 indicates that while the number of hydrated water molecules was commonly thought to be an integer, frequently that integer

was determined to differ from 6, particularly after de Forcrand had proposed his method.

The method considers the equilibrium of gas and  $n$  mol of liquid water (or ice) with hydrates on either side of the ice point:



Equation 4.14 for Lw–H–V equilibrium may be subtracted from Equation 4.15 for I–H–V equilibrium at quadruple point Q<sub>1</sub> (approximately 273 K), with the result of the number of moles of liquid water converted to ice:



where  $\Delta H_3 = \Delta H_1 - \Delta H_2$ .

Because the enthalpy of fusion ( $\Delta H_f$ ) of water is well known,  $\Delta H_3$ , the difference in the  $\Delta H$  values of Equations 4.14 and 4.15, may be divided by the heat of fusion of ice ( $\Delta H_f$ ) to obtain  $n$ , the number of moles of water (or ice) converted to hydrates.

The de Forcrand method has been found to be much more accurate than Villard's Rule. One reason for its accuracy is related to the determination of  $\Delta H_1$  and  $\Delta H_2$  from three-phase (Lw–H–V or I–H–V) equilibrium measurements of pressure and temperature via the Clapeyron equation:

$$\frac{dP}{dT} = \frac{\Delta H}{T\Delta V} \quad (4.17)$$

where  $\Delta H$  may be taken as the enthalpy change in either Equation 4.14 or 4.15,  $\Delta V$  is the corresponding volume change, and  $P$  and  $T$  are the phase equilibrium points along the appropriate three-phase line.

#### **Example 4.7: Hydration Number from Pressure–Temperature Data for Lw–H–V and I–H–V**

Sortland and Robinson (1964) measured the formation conditions of sulfur hexafluoride hydrates from 264 to 297 K. Using the Clapeyron equation with their data they determined values of  $\Delta H_1 = 29,570$  cal/gmol and  $\Delta H_2 = -5140$  cal/gmol. When these two values are added and the result is divided by the molar heat of fusion of water (1435.3 cal/gmol) a value of 17.02 gmol H<sub>2</sub>O per gmol SF<sub>6</sub> is obtained in the hydrate. This value is significantly different from that of Villard's Rule, and indicates that the SF<sub>6</sub> molecules essentially fill all of the large cavities in structure II hydrate. If each of the large cavities in structure II were filled, the ratio would be

exactly 17 (=136 water molecules/8 cavities). Note that most natural gases fill both cavities and thus have a lower hydration number that is approximated by Villard's Rule.

---

This indirect method avoids problems of metastability and occlusion in the direct method because the  $P$ - $T$  measurements are at equilibrium and they are not dependent on the amounts of each phase present. The question about the validity of the method centers on the validity of the Clapeyron equation to the three-phase hydrate equilibrium, as discussed in the following section.

Table 4.10 shows the literature values for hydrate numbers, all obtained using de Forcrand's method of enthalpy differences around the ice point. However, Handa's values for the enthalpy differences were determined calorimetrically, while the other values listed were determined using phase equilibrium data and the Clausius–Clapeyron equation. The agreement appears to be very good for simple hydrates. Note also that hydrate filling is strongly dependent on

---

**TABLE 4.10**  
**Hydration Number ( $M \cdot nH_2O$ ) for Simple Hydrates of Natural Gas Components from Handa (1986a,b)**

Component	<i>n</i>	Reference
Methane	6.00	Handa (1986a,b)
	5.99	Circone et al. (2006)
	5.77	Glew (1962)
	7.00	Roberts et al. (1941)
	7.18	Deaton and Frost (1946)
	6.00	Galloway et al. (1970)
	7.4	de Roo et al. (1983)
	6.3	de Roo et al. (1983)
Ethane	7.67	Handa (1986a,b)
	7.00	Roberts et al. (1941)
	8.25	Deaton and Frost (1946)
	8.24	Galloway et al. (1970)
Propane	17.0	Handa (1986a,b)
	5.7	Miller and Strong (1946)
	17.95	Deaton and Frost (1946)
	18.0	Knox et al. (1961)
	17.0	Cady (1983a)
Isobutane	17.0	Handa (1986b)
	17.1	Uchida and Hayano (1964)
	17.5	Rouher and Barduhn (1969)

---

pressure and temperature, so exact comparisons can only be made at identical conditions.

#### 4.6.2.2 Hydration numbers by the Miller and Strong method

After de Forcrand's Clapeyron, and Handa's methods, a third method for the determination of hydrate number, proposed by Miller and Strong (1946), was determined to be applicable when simple hydrates were formed from a solution with an inhibitor, such as a salt. They proposed that a thermodynamic equilibrium constant  $K$  be written for the physical reaction of Equation 4.14 to produce 1 mol of guest M, and  $n$  mol of water from 1 mol of hydrate. Writing the equilibrium constant  $K$  as multiple of the activity of each product over the activity of the reactant, each raised to its stoichiometric coefficient, one obtains:



where  $M \cdot (H_2O)_n \equiv$  hydrate (H)

$$K = \frac{(a_M)(a_W)^n}{a_H} \quad (4.18)$$

The thermodynamic reaction equilibrium constant  $K$ , is only a function of temperature. In Equation 4.18,  $a_M$ , the activity of the guest in the vapor phase, is equal to the fugacity of the pure component divided by that at the standard state, normally 1 atm. The fugacity of the pure vapor is a function of temperature and pressure, and may be determined through the use of a fugacity coefficient. The method also assumes that  $a_H$ , the activity of the hydrate, is essentially constant at a given temperature regardless of the other phases present.

The activity of water  $a_W$  in Equation 4.18 is normally taken as unity disregarding the solubility of the gas. At a given temperature, if an inhibitor such as a salt is present, the activity of the water decreases and the activity of the gas must increase in order to maintain a constant product  $K \cdot a_H$  at that temperature. Thus writing a second equation for the formation of a hydrate from an inhibited liquid we get

$$a_M \cdot a_W^n = K \cdot a_H \quad \text{without the inhibitor} \quad (4.18a)$$

and

$$a'_M \cdot a''_W = K \cdot a_H \quad \text{with the inhibitor} \quad (4.19)$$

Subtracting Equation 4.19 from Equation 4.18a, with the right sides constant, one may replace the activity of the guest M with its fugacity (if the same standard

state fugacity is used for both activities) to obtain

$$f_M \cdot a_W^n = f'_M \cdot a'_W^n \quad (4.20)$$

Recalling that the  $(')$  denotes the presence of an inhibitor, Equation 4.20 may be rearranged to obtain the hydrate number  $n$  as

$$n = \frac{\ln(f/f')}{\ln(a'/a)} \quad (4.21)$$

In Equation 4.21, the activity of pure water ( $a$ ) is unity and the activity of the water with the inhibitor ( $a'$ ) is the product of the water concentration ( $x_W$ ) and the activity coefficient ( $\gamma_W$ ). The water concentration is known and the activity coefficient is easily obtained from colligative properties for the inhibitor, such as the freezing point depression. For instance the activity of water in aqueous sodium chloride solutions may be obtained from Robinson and Stokes (1959, p. 476) or from any of several handbooks of chemistry and physics.

With the above data, Equation 4.21 indicates that the hydrate number  $n$  may be obtained from a measurement of the increase of the hydrate pressure with an inhibitor present at a given temperature. The fugacity may be calculated for a pure component from any of a number of thermodynamic methods given a temperature and pressure. Only in the case of a pure ideal gas (very low pressure or very high temperature) may the fugacities be replaced with the pressure itself.

It should be noted that this method contains several key assumptions, as follows:

1. The occupation of the hydrate does not change over the region of pressure and temperature considered.
2. The equilibrium constant  $K$  does not change when the inhibitor is added to the aqueous fluid, but it is only a function of temperature.
3. The activity of the hydrate phase is constant at a given temperature regardless of the other phases present.
4. The vapor presence of any component other than the hydrate former may be neglected, including any water or inhibitor present in the liquid.
5. The aqueous phase without inhibitor is pure water.

Exceptions may be found to the above assumptions and consequently the method might be expected to be more limited than the de Forcand method presented in Section 4.6.2.1. On the other hand, the de Forcand method requires more data. Rouher and Barduhn (1969) indicate that better results are achieved with the Miller and Strong method when NaCl solutions are in the range between 5 and 15 wt%.

Patil (1987) determined the hydrate number of simple propane hydrates to be 18.95 by the de Forcand method; using the Miller and Strong method he obtained hydrate numbers of 19.20, 19.95, and 19.89 for NaCl solutions of 3, 5, and

10 wt%, respectively. Wilms and van Haute (1973) presented the mathematically correct version of the Miller and Strong method, which eliminates some of the above assumptions, together with the statistical thermodynamic method of the following chapter. Wilms and van Haute suggest the Miller and Strong equations to be a special case of a more rigorous method.

#### 4.7 SUMMARY AND RELATIONSHIP TO CHAPTERS WHICH FOLLOW

The object of this chapter is to provide the reader with a qualitative understanding of hydrate phase equilibrium. Such an understanding implies a historical overview, which also provides successive approximations to hydrate phase equilibrium in terms of accuracy. The accuracy of three-phase prediction is given below in the order of increasing accuracy:

1. For pure components, use semilogarithmic interpolation between quadruple points  $Q_1$  and  $Q_2$ .
2. For pure components, use Antoine's equation with constants given in [Table 4.1](#).
3. For mixtures, use the gas gravity method.
4. For mixtures, use the  $K_{vsi}$  method, as the most accurate method of this chapter.

In the following chapter, the most accurate method available is discussed for the determination of hydrate equilibrium—that of statistical thermodynamics. The consideration of this method ties the macroscopic phase equilibrium, such as has been discussed qualitatively in the present chapter, to the microscopic structure discussed in [Chapter 2](#).

The bridging of the microscopic and macroscopic phenomena is satisfying both from a theoretical and from a pragmatic standpoint. Mathematical bridges between the microscopic and macroscopic domains are the major focus of [Chapter 6](#). Applications of the concepts of this chapter are also found in the final two chapters. Hydrates in the earth provide natural examples of phase equilibrium as detailed in [Chapter 7](#). Applications to artificial hydrates and their problems in flow lines are presented in [Chapter 8](#).

#### REFERENCES

- Austvik, T., Hustvedt, E., Meland, B., Berge, L., Lysne, D., "Tommeliten Gamma Field Hydrate Experiments," presented at *Seventh International Conference on Multiphase Production*, BHRA Group Conf. Ser. Publication 14, Cannes, June 7–9 (1995).
- Bansal, V., *Kinetic Study of Clathrate Hydrates*, M.S. Thesis, T-4545, Colorado School of Mines, Golden, CO, January (1994).
- Bansal, V., Christiansen, R.L., Sloan, E.D., "Influence of Guest Vapor–Liquid Critical Point on Hydrate Formation Conditions," *AICHE J.*, **39**(10), 1735 (1993).

- Barrer, R., Edge, A.V.J., *Proc. R. Soc. (London) A*, **300** (1967).
- Barrer, R.M., *Nature*, **183**, 463 (1959).
- Barrer, R.M., Stuart, W.I., *Proc. R. Soc. (London) A*, **243**, 172 (1957).
- Becke, P., Kessel, D., Rahimian, I., "Influence of Liquid Hydrocarbons on Gas Hydrate Equilibrium," SPE 25032, in *Proc. Europ. Petrol Conf. Cannes*, Nov. 16–18 (1992).
- Ben-Naim, A., *Hydrophobic Interaction*, Plenum Press, New York (1980).
- Berecz, E., Balla-Achs, M., *Gas Hydrates, Studies in Inorganic Chemistry*, Elsevier, New York, **411**, p. 343 (1977, English Translation 1983).
- Besnard, G., Song, K.Y., Hightower, J.W., Kobayashi, R., Elliot, D., Chen, R., "New Method of Temperature-Ramping, Isobaric Experiments to Study the Hydrate Formation and Composition," in *Proc. 213th ACS National Meeting*, San Francisco, CA, April 13–17, **42**(2), 551 (1997).
- Bourrie, M.S., Sloan, E.D., *Gas Proc. Assoc. Res. Rep.*, **100** (1986).
- Brown, G.G., *Trans AIME*, **160**, 65 (1945).
- Bucklin, R.W., Toy, K.G., Won, K.W., "Hydrate Control of Natural Gas Under Arctic Conditions Using TEG," in *Proc. Gas Conditioning Conference*, Norman, OK, (1985).
- Cady, G.H., *J. Phys. Chem.*, **85**, 4437 (1983a).
- Cady, G.H., *J. Chem. Ed.*, **60**, 915 (1983b).
- Carson, D.B., Katz, D.L., *Trans. AIME*, **146**, 150 (1942).
- Circone, S., Kirby, S.H., Stern, L.A., *J. Phys. Chem. B*, **110**(16), 8232 (2006).
- de Forcrand, R., *Compt. Rend.*, **135**, 959 (1902).
- de Roo, J.L., Peters, C.J., Lichtenhaler, R.N., Diepen, G.A.M., *AIChE J.*, **29**, 651 (1983).
- Deaton, W.M., Frost, E.M., Jr., *Gas Hydrates and their Relation to the Operation of Natural-Gas Pipe Lines*, U.S. Bureau of Mines Monograph 8, p. 101 (1946).
- Dickens, G.D., Quinby-Hunt, M.S., *J. Geophys. Res.*, **102**, 773 (1997).
- Franks, F., in *Water: A Comprehensive Treatise* (Franks, F., ed.) Plenum Press, New York, **2**, Chapter 1 (1973).
- Galloway, T.J., Ruska, W., Chappellear, P.S., Kobayashi, R., *Ind. Enq. Chem. Fundam.*, **9**, 237 (1970).
- Gibbs, J.W., *The Collected Works of J. Willard Gibbs, Thermodynamics*, Yale University Press, New Haven, CT, **I**, pp. 55–353 (1928).
- Gjertsen, L., Austvik, T., Urdahl, O., in *Proc. Second International Conference on Natural Gas Hydrates* (Monfort, J.P., ed.), Toulouse, June 2–6, p. 155 (1996).
- Glew, D.N., *J. Phys. Chem.*, **66**, 605 (1962).
- Hammerschmidt, E.G., *Ind. Eng. Chem.*, **26**, 851 (1934).
- Hammerschmidt, E.G., *Gas*, **15**(5), 30 (1939).
- Handa, Y.P., *J. Chem. Thermo.*, **18**, 891 (1986a).
- Handa, Y.P., *Calorimetric Studies of Laboratory Synthesized and Naturally Occurring Gas Hydrates*, paper presented at AIChE 1986 Annual Meeting Miami Beach, Nov 2–7 (1986b).
- Handa, Y.P., *J. Phys. Chem.*, **94**, 2652 (1990).
- Harmens, A., Sloan, E.D., *Can. J. Chem. Eng.*, **68**, 151 (1990).
- Holder, G.D., *Multi-Phase Equilibria in Methane–Ethane–Propane–Water Hydrate Forming Systems*, Ph.D. Thesis, University of Michigan, University Microfilms No. 77-7939, Ann Arbor, MI 48106, (1976).
- Huo, Z., Hester, K., Miller, K.T., Sloan, E.D., *AIChE J.*, **49**, 1300 (2003).

- Jacoby, R.H., "Vapor–Liquid Equilibrium Data for Use of Methanol in Preventing Gas Hydrates," in *Proc. Gas Hydrocarbon. Control Conference*. University of Oklahoma, Norman, OK (1953).
- Jhaveri, J., Robinson, D.B., *Can. J. Chem. Eng.*, **43**, 75 (1965).
- Kamath, V.A., *Study of Heat Transfer Characteristics during Dissociation of Gas Hydrates in Porous Media*, Ph.D. Dissertation, University of Pittsburgh, University Microfilms No. 8417404, Ann Arbor, MI (1984).
- Katz, D.L., *Trans AIME*, **160**, 140 (1945).
- Katz, D.L., *J. Petrol Tech.*, **24**, 557 (1972).
- Katz, D.L., Cornell, D., Kobayashi, R., Poettmann, F.H., Vary, J.A., Elenbaas, J.R., Weinaug, C.F., *Handbook of Natural Gas Engineering*, McGraw-Hill, New York, p. 802, (1959).
- Knox, W.G., Hess, M., Jones, G.E., Smith, H.B., *Chem. Eng. Prog.*, **57**(2), 66 (1961).
- Kobayashi, R., *Vapor–Liquid Equilibrium in Binary Hydrocarbon–Water Systems*, Ph.D. Dissertation, University of Michigan, University Microfilms No. 3521, Ann Arbor, MI (1951).
- Kobayashi, R., Katz, D.L., *Trans AIME*, **186**, 66 (1949).
- Kobayashi, R., Katz, D.L., *Trans AIME*, **204**, 51 (1955).
- Kobayashi, R., Song, K.Y., Sloan, E.D., in *Petroleum Engineering Handbook* (Bradley, H.B., ed.) Society of Petrol Eng., Richardson, TX, Chapter 25 (1987).
- Koga, K., *Study of Stability and Dynamics of Clathrate Hydrates and Supercritical Fluids*, Ph.D. Thesis, Kyoto University, Japan (1995).
- Koga, K., Tanaka, H., *J. Chem. Phys.*, **104**, 263 (1996).
- Koga, K., Tanaka, H., Nakanishi, K., *J. Chem. Phys.*, **101**, 3127 (1994a).
- Koga, K., Tanaka, H., Nakanishi, K., *Mol. Simul.*, **12**(3–6), 241 (1994b).
- Koretsky, M.D., *Engineering and Chemical Thermodynamics*, John Wiley, Hoboken, NJ, 2004.
- Kuhs, W., Chazallon, B., Radaelli, P., Pauer, F., Kipfstuhl, J., in *Proc. Second International Conference on Natural Gas Hydrates* (Monfort, J.P., ed.) Toulouse, France, June 2–6, p. 9 (1996).
- Loh, J., Maddox, R.N., Erbar, J.H., *Oil Gas J.*, **96**(May), 16, (1983).
- Makogon, T.Y., Mehta, A.P., Sloan, E.D., *J. Chem. Eng. Data*, **41**, 315 (1996).
- Makogon, Y.F., *Hydrates of Natural Gas*, Moscow, Nedra, Izadatelstro, p. 208 (1974 in Russian) Transl W.J. Cieslesicz, PennWell Books, Tulsa, Oklahoma p. 237 in Russian, (1981 in English).
- Mann, S.L., McClure, L.M., Poettmann, F.H., Sloan, E.D., "Vapor–Solid Equilibrium Ratios for Structure I and Structure II Natural Gas Hydrates," in *Proc. 68th Annual Gas Processing Association Convention*, San Antonio, TX, March 13–14 (1989).
- McKetta, J.J., Wehe, A.H., *Petroleum Refiner*, **37**, 153 August (1958).
- Mehta, A.P., *A Thermodynamic Investigation of Structure H Clathrate Hydrates*, Ph.D. Thesis, Colorado School of Mines, Golden, CO (1996).
- Mehta, A.P., Ripmeester, J., "Structural Characterization of Hydrate Formation in Black Oil and Gas Condensate Systems," in *Proc. Fourth International Conference on Gas Hydrates*, Yokohama, Japan, May 19–23, 580 (2002).
- Mehta, A.P., Sloan, E.D., in *Proc. Second International Conference on Natural Gas Hydrates* (Monfort, J.P., ed.), Toulouse, France, June 2–6, p. 1 (1996a).
- Mehta, A.P., Sloan, E.D., "Structure H Hydrates: Implications for the Petroleum Industry," in *Proc. 1996 Annual Technical Conference*, SPE 36742, 607 Denver, CO, October 6–9 (1996b).

- Menten, P.D., Parrish, W.R., Sloan, E.D., *Ind. Eng. Chem. Proc. Des. Dev.*, **20**, 399 (1981).
- Miller, B., Strong, E.R., *Am. Gas Assoc. Monthly*, **28**(2), 63 (1946).
- Nakayama, H., Hashimoto, M., *Bull. Chem. Soc. Japan*, **53**, 2427 (1980).
- Nakayama, H., Brouwer, D.H., Handa, Y.P., Klug, D.D., Tse, J.S., Ratcliffe, C.I., Zhu, X., Ripmeester, J.A., "Methanol: Clathrate Hydrate Former or Inhibitor?" in *Proc. 213th ACS National Meeting*, San Francisco, CA, April 13–17, **42**(2), 516 (1997).
- Nelson, K., *Hydrocarbon Process.*, **September**, 161 (1973).
- Ng, H.-J., Chen, C.-J., *Gas Proc. Assoc. Res. Rep.* **149**, March (1995).
- Ng, H.-J., Robinson, D.B., *AIChE J.*, **23**, 477 (1977).
- Ng, H.-J., Robinson, D.B., *Gas Proc. Assoc. Res. Rep.*, **66**, April (1983).
- Nielsen, R.B., Bucklin, R.W., *Hydrocarbon Process.*, April, 71, (1983).
- Nixdorf, J., Oellrich, L., in *Proc. Second International Conference on Natural Gas Hydrates* (Monfort, J.P., ed.) Toulouse, France, June 2–6, 17 (1996).
- Noaker, L.J., Katz, D.L., *Trans AIME*, **201**, 237 (1954).
- Olds, R.H., Sage, B.H., Lacey, W.N., *Ind. Enq. Chem.*, **34**, 1223 (1942).
- Patil, S.L., *Measurements of Multiphase Gas Hydrates Phase Equilibria: Effect of Inhibitors and Heavier Hydrocarbon Components*, M.S. Thesis, University of Alaska (1987).
- Patwardhan, V.S., Kumar, A., *AIChE J.*, **32**, 1419 (1986).
- Pieroen, A.P., *Rec. Trav. Chim.*, **74**, 995 (1955).
- Poettmann, F.H., *Hydrocarbon Proc.*, **63**(6), 111 (1984).
- Pohlman, J.W., Canuel, E.A., Chapman, N.R., Spence, G.D., Whiticar, M.J., Coffin, R.B., *Org. Geochem.*, **36**, 703 (2005).
- Records, J.R., Seely, D.H., Jr., *Trans AIME*, **192**, 61 (1951).
- Ripmeester, J.A., Tse, J.A., Ratcliffe, C.I., Powell, B.M., *Nature*, **325**, 135 (1987).
- Ripmeester, J.A., Ratcliffe, C.I., *Inclusion Compounds* (Atwood, J.L., Davies, J.E.D., et al., eds.), **5**, Oxford University Press (1991).
- Roberts, O.L., Brownscombe, E.R., Howe, L.S., *Oil Gas J.*, **39**(30), 37 (1940).
- Roberts, O.L., Brownscombe, E.R., Howe, L.S., Ramser, H., *Petrol. Eng.*, **3**, 56 (1941).
- Robinson, D.B., Mehta, B.R., *J. Can. Petr. Tech.*, **10**, 33 (1971).
- Robinson, R.A., Stokes, R.H., *Electrolyte Solutions*, Butterworths Scientific Publications, London (1959).
- Rouher, O.S., Barduhn, A.J., *Desalination*, **6**, 57 (1969).
- Sassen, R., MacDonald, I.R., *Org. Geochem.*, **22**(6), 1029 (1994).
- Scauzillo, F.R., *Chem. Eng. Prog.*, **52**, 324 (1956).
- Servio, P., Englezos, P., *J. Chem. Eng. Data*, **47**, 87 (2002).
- Skinner, W., Jr., *The Water Content of Natural Gas at Low Temperatures*, M.S. Thesis, University of Oklahoma, Norman, OK (1948).
- Skovborg, P., Rasmussen, P., *Chem. Eng. Sci.*, **49**, 1131 (1994).
- Sloan, E.D., in *Proc. 63rd Annual Convention of Gas Processors Association*, **63**, 163, San Antonio, TX, March 15 (1984).
- Sloan, E.D., Fleyfel, F., *Fluid Phase Equilib.*, **76**, 123 (1992).
- Sloan, E.D., Fleyfel, F., *Fluid Phase Equilib.*, **96**, 233 (1994).
- Sloan, E.D., Khouri, F.M., Kobayashi, R., *Ind. Eng. Chem. Fundam.*, **15**, 318 (1976).
- Sloan, E.D., Sparks, K.A., Johnson, J.J., Bourrie, M.S., *Fluid Phase Equilib.*, **29**, 233 (1986).
- Sloan, E.D., Sparks, K.A., Johnson, J.J., *Ind. Eng. Chem. Res.*, **26**, 1173 (1987).
- Song, K.Y., Feneyrou, G., Fleyfel, F., Martin, R., Levois, J., Kobayashi, R., *Fluid Phase Equilib.*, **128**, 249 (1997).
- Song, K.Y., Kobayashi, R., *Ind. Eng. Chem. Fund.*, **21**, 391 (1982).

- Song, K.Y., Kobayashi, R., *SPE Form. Eval.*, December, 500 (1987).
- Song, K.Y., Kobayashi, R., *Fluid Phase. Equilib.*, **95**, 281 (1994).
- Sortland, L.D., Robinson, D.B., *Can. J. Chem. Eng.*, **42**, 38 (1964).
- Stange, E., Majeed, A., Overa, S., "Experiments and Modeling of the Multiphase Equilibrium of Inhibition of Hydrates," in *Proc. 68th Annual Gas Processors Association Convention*, San Antonio, TX, March 13–14, 1989.
- Svartas, T.M., "Overview of Hydrate Research at Rogalands-Forsknings," presented at *BHRA Conference on Operational Consequences of Hydrate Formation and Inhibition Offshore*, Cranfield, UK, November 3, (1988).
- Thakore, J.L., Holder, G.D., *Ind. Eng. Chem. Res.*, **26**, 462 (1987).
- Tohidi, B., Danesh, A., Burgass, R., Todd, A., SPE28478, in *Proc. SPE 69th Annual Technical Conference*, New Orleans, September 25–28, 157 (1994).
- Tohidi, B., Ostergaard, K.K., Danesh, A., Todd, A.C., Burgass, R.W., *Can. J. Chem. Eng.*, **79**, 384 (2001).
- Toplak, G.J., *Solubilities of Hydrocarbon Gas Mixtures in Distilled Water Near Hydrate Forming Conditions*, M.S. Thesis, University of Pittsburgh, PA (1989).
- Townsend, F.M., Reid, L.S., *Hydrate Control in Natural Gas Systems*, Laurance Reid Associates, Inc., P.O. Box 1188, Norman, OK 73070 (1978).
- Uchida, T., Hayano, I., *Rep. Govt. Chem. Ind. Res. Inst., Tokyo*, **59**, 382 (1964).
- Unruh, C.H., Katz, D.L., *Trans AIME*, **186**, 83 (1949).
- van der Waals, J.H., Platteeuw, J.C., "Clathrate Solutions," *Adv. Chem. Phys.*, **2**, 1 (1959a).
- van der Waals, J.H., Platteeuw, J.C., *Nature*, **183**(4659), 462 (1959b).
- van Hinsberg, M.G.E., Scheerboom, M.I.M., Schouten, J.A., *J. Chem. Phys.*, **99**, 752 (1993).
- van Hinsberg, M.G.E., Schouten, J.A., "The Phase Diagram of Nitrogen Clathrate Hydrate," *Am. Inst. Phys.*, **309**, 271 (1994).
- Verma, V.K., *Gas Hydrates from Liquid Hydrocarbon-Water Systems*, Ph.D. Thesis, University of Michigan, University Microfilms No. 75-10,324, Ann Arbor, MI (1974).
- Villard, P., *Compt. Rend.*, **120**, 1262 (1895).
- Wallqvist, A., *Chem. Phys. Lett.*, **182**(3,4), 237 (1991).
- Wallqvist, A., *J. Chem. Phys.*, **96**, 5377 (1992).
- Wierzchowski, S.A., Monson, P.A., *Ind. Eng. Chem. Res.*, **45**, 424 (2006).
- Wilcox, W.I., Carson, D.B., Katz, D.L., *Ind. Eng. Chem.*, **33**, 662 (1941).
- Wilms, D.A., van Haute, A.A., *Fourth International Symposium on Fresh Water From the Sea*, **3**, 477 (1973).
- Woolridge, P.J., Richardson, H.H., Devlin, J.P., *Chem. Phys.*, **87**, 4126 (1987).
- Wu., B.-J., Robinson, D.B., Ng, H.-J., *J. Chem. Thermodyn.*, **8**, 461 (1976).
- Yamane, K. Aya, I., "Solubility of Carbon Dioxide in Hydrate Region at 30 MPa," in *Proc. International Conference on Technology for Marine Environment Preservation*, Tokyo, Sept 24–29, **2**, 911 (1995).
- Yamanlar, S., Poettmann, F.R., Sloan, E.D., *Hydrocarbon Process.*, 155(September) (1991).
- Yousif, M., Austvik, T., Berge, L., Lysne, D., in *Proc. Second International Conference on Natural Gas Hydrates* (Monfort, J.P., ed.) Toulouse, France, June 2–6, 291 (1996).